PHYSICS-ORIENTED STATISTICAL MODELING, SIMULATION AND OPTIMIZATION

J.W. Bandler, R.M. Biernacki, Q. Cai, S.H. Chen,
S. Ye and Q.J. Zhang

SOS-91-6-R

September 1991

PHYSICS-ORIENTED STATISTICAL MODELING, SIMULATION AND OPTIMIZATION

J.W. Bandler*, R.M. Biernacki*, Qian Cai*, S.H. Chen*, S. Ye** and Q.J. Zhang+

Abstract We contribute herein to the effective utilization of physics-, geometry- and process-related parameters for yield-driven microwave device modeling and circuit design. We address physics-based modeling of MESFETs from the point of view of efficient performance prediction and robust parameter extraction. We have developed a new formula to approximate the behaviour of electron drift velocity versus electric field. We present a novel integration of the resulting model into the harmonic balance simulation of nonlinear circuits, involving an efficient Newton update. We exploit this integration in gradient-based *FAST* (*F*easible *A*djoint *S*ensitivity *T*echnique) circuit optimization. To support yield-driven circuit optimization we present a relevant physics-based statistical modeling methodology. Our statistical implementations use models originated by Ladbrooke and Khatibzadeh and Trew. We embed these physics-based device models in the yield optimization of MMICs using appropriate multidimensional statistical distributions. Quadratic approximation of responses and gradients suitable for yield optimization is discussed. We verify our theoretical contributions and exemplify our computational results using built-in and user-programmable modeling capabilities of the new CAE system OSA90/hope as well as HarPE. In this context, we report on results of device modeling using a field-theoretic nonlinear device simulator.

This work was supported in part by the Natural Sciences and Engineering Research Council of Canada under Grants STR0040923, OGP0007239 and OGP0042444 and in part by Optimization Systems Associates Inc.

* J.W. Bandler, R.M. Biernacki, Q. Cai and S.H. Chen are with the Simulation Optimization Systems Research Laboratory and the Department of Electrical and Computer Engineering, McMaster University, Hamilton, Canada L8S 4L7. J.W. Bandler, R.M. Biernacki, S.H. Chen are also with Optimization Systems Associates Inc., P.O. Box 8083, Dundas, Ontario, Canada L9H 5E7.

** S. Ye is now with Optimization Systems Associates Inc., P.O. Box 8083, Dundas, Ontario, Canada L9H 5E7.

+ Q.J. Zhang is now with the Department of Electronics, Carleton University, Ottawa, Canada K1S 5B6.

I. INTRODUCTION

We believe that microwave computer-aided engineering (CAE) technology must address physics-based circuit optimization directly linking geometrical, material and process-related parameters, or simply, physical parameters, with system performance and production yield, etc. Field theory, circuit theory and system theory need to be integrated into hierarchically structured, mathematically-oriented computer-aided design (CAD) systems for process-oriented linear, nonlinear and statistical microwave circuit simulation and design.

For active microwave circuit design the effectiveness of modern CAD methods relies heavily on accurate device models. Approaches to device modeling have been developed and a variety of models have been implemented into circuit simulators for such purposes as small- and large-signal circuit design. Generally, the methods for device modeling can be classified into two categories: equivalent circuit-based models (ECM) and physics-based models (PBM).

ECM modeling assumes an equivalent circuit model to simulate the external behaviour of the device under consideration. The model consists of linear and nonlinear circuit elements to represent device characteristics. Empirical equations are devised *a priori* for those nonlinear circuit elements. The determination of the ECM parameters usually depends on accurate parameter extraction from measured or simulated DC and AC data. For example, ECMs for FETs, including small-signal and nonlinear large-signal ECMs [1-5], have been widely used in microwave CAD. The models are normally characterized through DC, S-parameter and/or large-signal measurement data after the device is fabricated [6-7]. ECMs enjoy high computational efficiency and can be easily implemented into circuit simulators. They have been the foundation of pre-MMIC (monolithic microwave integrated circuits) CAD and continue to dominate today's microwave simulators. They are easily understood by microwave engineers. However, there is no obvious relationship between ECM parameters and device physical parameters. Also, since the model parameters are usually identified after device fabrication, they have limited extrapolative or statistically meaningful forecasting abilities. This opens the door to PBM modeling.

PBM modeling attempts to solve the fundamental device equations, describing device characteristics in terms of physical parameters such as gate length, channel thickness, doping profile, etc. Circuit design can then be considered at the device parameter level. In other words, the design variables can be directly the device geometrical, material and process-related parameters [8]. Therefore, PBM should be very effective in terms of predictability and first-time success in the development of microwave integrated circuits (MICs) and MMICs.

Efficient microwave nonlinear circuit analysis has been a subject of serious research for a long time. Its importance has resurged by the development of MICs and MMICs where active devices are components critical to performance. The analysis of nonlinear circuits is much more complicated than that of linear circuits. Simulation of nonlinear circuits can be in the time-domain, frequency-domain and mixed frequency/time-domains [9].

Time-domain methods try to solve the circuit equations entirely in the time-domain using numerical methods. There are three major time-domain simulation techniques [9]: direct methods [10-15], associated discrete circuit model approaches [10,16] and shooting methods [17-22]. Frequency-domain methods, recently reviewed by Steer, Chang and Rhyne [23] attempt to analyze nonlinear circuits entirely in the frequency-domain. Functional expansions enable the frequency components of the output spectrum to be calculated directly from the input spectrum. Frequency-domain methods such as power series expansion analysis [24-27], Volterra series analysis [28-33] and spectral balance analysis [34-36], have been used successfully for the analysis of microwave nonlinear circuits [37-44].

Mixed frequency/time-domain methods simulate nonlinear circuits in both frequency and time domains: the harmonic balance (HB) technique [45-51], extensively reviewed by Gilmore and Steer [9,52], and the waveform balance (or sample balance) technique. The HB technique is an efficient tool for the simulation of steady-state responses of nonlinear microwave circuits [53-57]. The waveform balance approach can be considered a dual to the HB method. It has been used for solving nonlinear pumping problems [58] and for nonlinear modeling and verification of MMIC amplifiers

[59].

Nonlinear circuit optimization requires efficient nonlinear circuit simulation. It has become feasible because of the efficiency of the HB method. Applications of optimization employing the HB method have included large-signal FET model parameter extraction [7], nonlinear circuit design [60-62] and nonlinear circuit yield optimization [63], although most of the developments have been directed to ECMs. Active and passive elements are explicitly represented through their equivalent circuits. The direct treatment of the effects of physical parameters of devices in MMICs (e.g., a MESFET) on overall circuit performance has been studied by a number of researchers [8,64-71]. One of the most significant benefits of the PBMs over the ECMs is the feasibility of directly optimizing controllable/designable parameters of the passive and active devices for low noise, high power, high yield, etc.

Statistical device modeling is a prerequisite for accurate yield-driven or cost-driven circuit analysis and optimization [72,73]. The model statistics originate from random variations of geometrical, material and process-related parameters during manufacturing. Those random variations result in complicated distributions and correlations of device responses. The aim of statistical device modeling is to provide tools for generating random device outcomes which can represent the actual distribution of the device responses. Statistical modeling has been seriously studied for passive devices, bipolar junction transistors (BJT), metal-oxide semiconductor (MOS) and complementary metal-oxide semiconductor (CMOS) circuits for more than a decade [74-82]. Statistical modeling techniques have also been applied to microwave devices [73,83-86].

With the rapid progress of GaAs fabrication technology, MMICs are becoming more and more practical [87]. During the past two decades, hybrid microwave integrated circuits (HMICs) have been used in the microwave industry, where active and passive discrete components such as transistors, thin- or thick-film capacitors, inductors and resistors are connected on a dielectric substrate. In MMICs, all the active and passive components are fabricated on a common semi-insulating substrate. Post-production tuning of MMICs is restricted, and device replacement is not possible. In the

production of MMICs, circuits are manufactured in batches rather than individually. Random variations in the manufacturing process typically result in a portion of the circuits which do not meet the design specifications. Therefore, yield analysis and optimization is accepted as an indispensable part of the MMIC design methodology, since the yield significantly affects the cost of manufacturing. Yield optimization, which takes into account the manufacturing tolerances, model uncertainties, variations of the process parameters and environmental uncertainties, etc., has become an important tool to reduce cost.

Yield optimization techniques can be traced back to the early 1970s. Pioneering work was carried out by many researchers [88-92] and was advanced subsequently during the last two decades [93-118]. Yield optimization of nonlinear microwave circuits with statistically characterized devices has been seen in the literature, e.g., [63, 119, 120]. Purviance and Meehan [121] recently reviewed statistical analysis and design of microwave circuits. Many approaches developed for yield optimization are restricted to the circuit level: analyses employ ECMs. Statistical characteristics are then applied to circuit elements such as capacitors, inductors and resistors. There is doubt as to whether such an approach is capable of reflecting the actual statistical behaviour of the physical parameters. In MMICs, a change in one single physical parameter of a device may result in correlated changes in all elements of its equivalent circuit model. Furthermore, the resulting correlations may be very complicated and quite difficult to describe by ECMs. Therefore, conventional design methods at the circuit level are not suitable for yield optimization of MMICs. On the other hand, PBMs are more likely to provide reliable statistical behaviour because of the physical nature of the model. Consequently, meaningful results of yield optimization should be attainable [122-123].

State-of-the-art microwave circuit analysis and design requires comprehensive general-purpose CAD software to integrate device modeling, steady-state and transient circuit simulation, sensitivity analysis, statistical modeling and analysis, performance- and yield-driven design optimization, as well as physics-based and process-oriented circuit design within the same framework. In a recent review of the MIMIC (Microwave and Millimeter Wave Monolithic Integrated Circuits) Program's progress,

Cohen [69] emphasized open architecture CAD approaches. Different aspects of a CAD system, such as technology optimization, cell design, software modularity and adaptability, have been discussed [124-126].

With the rapid expansion of powerful UNIX-based workstations, development of such comprehensive CAD systems is increasingly realistic. For example, a new CAD software system OSA90/hope [127], created by Optimization Systems Associates, performs general linear and nonlinear circuit simulation and optimization, Monte Carlo analysis, accepts user-defined models using expressions and arbitrary topology in addition to its built-in device library, and accepts linear and nonlinear symbolic subcircuit definitions. OSA90/hope can interconnect separate external programs, providing users a secure opportunity to merge personal programs to exploit the system's built-in state of the art features.

In Section II, we present PBM modeling of MESFET. Nonlinear circuit analysis using PBMs integrated with the HB method is addressed in Section III. Circuit design exploiting gradient optimizers is presented in Section IV. Sections V and VI consider statistical modeling and yield optimization, respectively, using PBMs. Section VII briefly describes OSA90/hope, which has been used in addition to HarPE [128] to verify our theoretical contributions and exemplify our computational results. In this context, we present results of device modeling using a 2-dimensional nonlinear MESFET device simulator.

II. MESFET MODELING

The fundamental device equations for PBMs may be solved numerically and analytically. Numerical models typically employ finite-difference or finite-element techniques [129-134]. They play an important role in physical understanding of the device. They have, however, been hitherto regarded as cumbersome. Analytical PBM modeling can be traced back to the early pioneering work of Shockley [135] in 1952. He invented the JFET and developed a detailed analysis based on three major assumptions: constant mobility in the material, gradual channel approximation and abrupt

transition between the depletion region and the conducting channel [71]. His model was applicable to long gate devices operating in a non-saturated mode, and therefore is not suitable for modern high-frequency transistors. Shockley's analysis was improved subsequently by a number of researchers by including velocity saturation effects and nonuniform doping profile in the channel [136-141]. All these models are based on one-dimensional or quasi one-dimensional analysis. They are suitable for DC and small-signal AC operation with the devices restricted to large gate-length L to channel thickness a ratios. To eliminate these restrictions, a number of large-signal analytical models were proposed [142-145]. Large-signal analytical models try to solve the device equations with a minimum number of simplifying assumptions. These models offer a compromise between simulation efficiency and model accuracy. They are quite suitable for circuit design and optimization.

A. Basic Device Equations [144]

A simplified cross-section of the MESFET is shown in Fig. 1. A buffer layer is first grown on the semi-insulating (SI) substrate. This layer has a high resistivity and contains very few mobile electrons. It acts effectively as an extension of the SI substrate but protects the subsequently grown active layer from any deleterious effects due to the bulk substrate which could otherwise occur. An active layer is then grown onto the buffer layer. Source and drain ohmic contacts are planted into the active layer. A Schottky barrier is grown on the active layer between the source and drain contacts as the gate electrode. Following [144], the device model is formulated around the active region or "intrinsic" region as shown in Fig. 2. This region consists of the area of the channel directly under the gate electrode. All other regions of the device are modeled phenomenologically using external or "extrinsic" linear elements. The basic device equations in the active region are

$$\nabla^2\psi = -\frac{q}{\varepsilon}\left[N(y) - n(x, y)\right] \tag{1}$$

$$\boldsymbol{J} = -qn\upsilon + qD\nabla n \tag{2}$$

$$\nabla\cdot\boldsymbol{J} = q\frac{\partial n}{\partial t} \tag{3}$$

and

$$\boldsymbol{J}_t = \boldsymbol{J} + \varepsilon \frac{\partial \boldsymbol{E}}{\partial t} \tag{4}$$

where

$$\boldsymbol{E} = -\nabla\psi \tag{5}$$

is the electric field, ψ is the electrostatic potential, N the donor concentration in the channel, n the free-electron density, $\boldsymbol{v}$ the electron velocity, D the diffusion coefficient, $\boldsymbol{J}$ the conduction (drift + diffusion) current density, $\boldsymbol{J}_t$ the total (conduction + displacement) current density, q the electron charge, and ε the permittivity of the active layer material. It is assumed that $\boldsymbol{v}$ and $\boldsymbol{E}$ are codirectional, i.e.,

$$\boldsymbol{v} = -\mu(E)\boldsymbol{E} \tag{6}$$

where E is the magnitude of $\boldsymbol{E}$ and $\mu(E)$ is the field-dependent mobility. Among the basic device equations, (1) is Poisson's equation, and (3) is the current continuity equation. They contribute to a "drift-diffusion" PBM which characterizes the behaviour of the FET devices.

The active region is divided into three parts: a depletion region under the gate Schottky barrier where $n = 0$, a free channel region where $n = N_d$ and N_d is the doping density, and a transition region where n varies smoothly from zero to N_d [143]. The free electron density in the transition region may be approximated by a sinusoidal expression [142,143]

$$n(x, y) = N_d\left[1 - \alpha(x-\gamma)\right]\frac{1 + \cos\frac{\pi}{d_1}(y - d(x))}{2} \tag{7}$$

or by an exponential function [144]

$$n(x, y) = N(y)\left[1 + \gamma(x - L_1)\right]\left[1 - \frac{1}{1 + \exp\left(\frac{y - d(x)}{\lambda}\right)}\right] \tag{8}$$

where α, γ, L_1, d_1 and λ are the parameters to be determined by the boundary conditions and the bias. $d(x)$ can be thought of as an "effective depletion-layer width" [144]. With (7) or (8) the assumption of abrupt transition between the depletion region and the conducting channel is eliminated.

B. Velocity-Electric Field Dependence

The dependence of the electron drift velocity v on the electric field E is usually approximated by piecewise linear or quadratic functions as shown in Fig. 3, in which the negative differential mobility of GaAs is neglected [143,144]. An equation with a step function is used in [145] to approximate the negative differential mobility, though the calculated and the measured mobilities do not fit well.

Here we propose a new and more flexible formula to approximate the behaviour of the v-E relation in GaAs. Our formula is based on the quadratic function [144] shown in Fig. 3

$$v_1 = \begin{cases} v_s & E \geq 2E_c \\ \mu_0 E - \dfrac{v_s}{4E_c^2}E^2 & E < 2E_c \end{cases} \tag{9}$$

where v_s is the saturation velocity, μ_0 is the low field mobility, and E_c denotes the critical electric field and satisfies the relation

$$v_s = \mu_0 E_c \ . \tag{10}$$

We propose the term

$$v_2 = \frac{v_s}{C} B \left[\frac{\dfrac{E}{A} - C}{\left(\dfrac{E}{A}\right)^{\beta} + B} + \frac{C}{B} \right] \tag{11}$$

and associate it with v_1 by forming the v-E representation as

$$v = (1 - \alpha)v_1 + \alpha v_2 \tag{12}$$

where A, B, C, α and β are fitting parameters extracted to best fit measurement data.

The main advantages of (12) are that the negative differential mobility of the v-E curve can be accommodated and that it is easy to use in the model formulation. In Fig. 4 the v-E curve calculated by (12) with $v_s = 1.206\times10^5$m/s, $\mu_0 = 0.6625\text{m}^2/(\text{Vs})$, $\beta = 3.832$, A = 1.081×10^5V/cm, B = 68.9, C = 1.363 and $\alpha = 1.998$, is compared with the experimental data used by Chang and Day [145] and attributed to Ruch and Kino [146], and Houston and Evans [147]. We observe that the use of (12)

results in a very close fit to the experimental data.

C. Solution for the Potential Distribution

The general solution of Poisson's equation (1) can be represented by a linear superposition of two components of the form [142–144]

$$\psi = \psi_0 + \psi_1 \tag{13}$$

where ψ_0 is the Laplacian potential due to the impressed voltages on the electrodes. ψ_0 satisfies

$$\nabla^2\psi_0 = 0 \tag{14}$$

with the boundary conditions (see Fig. 2)

$$\psi_0(0, a) = 0 \tag{15a}$$

$$\psi_0(L, a) = v_0 \tag{15b}$$

$$\frac{\partial\psi_0(x, a)}{\partial y} = 0 \tag{15c}$$

$$\psi_0(x, 0) = 0 \ . \tag{15d}$$

ψ_1 is due to the space charge in the channel and satisfies

$$\nabla^2\psi_1 = -\frac{q}{\varepsilon}(N - n) \tag{16}$$

with the boundary conditions

$$\psi_1(0, a) = 0 \tag{17a}$$

$$\psi_1(L, a) = v_1 \tag{17b}$$

$$\frac{\partial\psi_1(x, a)}{\partial y} = 0 \tag{17c}$$

$$\psi_1(x, 0) = v_{gs} - V_{bi} \tag{17d}$$

where L and a are the gate length and channel thickness, respectively, V_{bi} is the built-in voltage of the gate Schottky contact, and v_{gs} is the applied intrinsic gate–source voltage. v_0 and v_1 are unknown fractions of v_{ds}, the applied intrinsic drain–source voltage, resulting from the boundary conditions (15b) and (17b) and must be solved for in order to determine the performance of the devices. Since $v_{ds} = v_1 + v_0$, it is sufficient to solve for v_1 only.

Khatibzadeh and Trew [144] showed that a simplified solution to (14) with the boundary

conditions (15a)–(15d) is

$$\psi_0(x, y) = \frac{v_0}{\sinh\left(\frac{\pi L}{2a}\right)} \sinh\left(\frac{\pi x}{2a}\right) \sin\left(\frac{\pi y}{2a}\right) \tag{18}$$

and the solution to (16) with the boundary conditions (17a)–(17d) can be expressed as

$$\psi_1(x, y) = \begin{cases} -\frac{q}{\varepsilon} F_1(d(x)) + \frac{v_1}{L} x & 0 \le x \le L_1 \\ -\frac{q}{\varepsilon} F_1(d_1) + \frac{v_1}{L} x + \frac{q}{\varepsilon} \gamma(x - L_1) F_2(d_1) & L_1 < x \le L \end{cases} \tag{19}$$

where

$$F_1(d(x)) = \int_y^a \int_z^a [1 - T(d(x), z)] N(z) dz dy$$

$$F_2(d_1) = \int_y^a \int_z^a T(d_1, z) N(z) dz dy$$

and

$$T(d(x), y) = 1 - \frac{1}{1 + \exp\left(\frac{y - d(x)}{\lambda}\right)} \tag{20}$$

is the transition function. d_1 is the depletion–layer width in the saturation region.

D. Improvement of Model Efficiency Under Uniform Doping

The solution for the potential ψ_1 in (19) involves two double integrations F_1 and F_2 which require substantial computational effort. However, it is necessary if the doping profile is arbitrary. We have observed that for uniform doping the efficiency of the model would be greatly improved if the transition function could be integrated analytically. We have, therefore, developed a transition function to approximate the transition function in (20), namely

$$T(d(x),\ y) = \begin{cases} \dfrac{1 + \cos\left[\pi \dfrac{y - d(x) - 3\lambda}{6\lambda}\right]}{2} & \text{if } d(x) - 3\lambda < y < d(x) + 3\lambda \\ 0 & \text{if } y \le d(x) - 3\lambda \\ 1 & \text{if } y \ge d(x) + 3\lambda \end{cases} \tag{21}$$

Our formulation is a modification of the transition function in [143] such that it provides a good approximation to the transition curve from (20). This improvement has been implemented in OSA90/hope [127] and our simulation experiments have shown that the simulation time can be reduced more than three times.

E. Intrinsic Currents

The gate, drain and source currents can be represented by the equations

$$i_g = i_{gc}(\boldsymbol{\phi},\ v_1(\boldsymbol{\phi},t),\ v_{gs}(\boldsymbol{\phi},t),\ v_{ds}(\boldsymbol{\phi},t),\ t) + \frac{\partial q_g(\boldsymbol{\phi},\ v_1(\boldsymbol{\phi},t),\ v_{gs}(\boldsymbol{\phi},t),\ v_{ds}(\boldsymbol{\phi},t),\ t)}{\partial t} \tag{22}$$

$$i_d = i_{dc}(\boldsymbol{\phi},\ v_1(\boldsymbol{\phi},t),\ v_{gs}(\boldsymbol{\phi},t),\ v_{ds}(\boldsymbol{\phi},t),\ t) + \frac{\partial q_d(\boldsymbol{\phi},\ v_1(\boldsymbol{\phi},t),\ v_{gs}(\boldsymbol{\phi},t),\ v_{ds}(\boldsymbol{\phi},t),\ t)}{\partial t} \tag{23}$$

$$i_s = i_{sc}(\boldsymbol{\phi},\ v_1(\boldsymbol{\phi},t),\ v_{gs}(\boldsymbol{\phi},t),\ v_{ds}(\boldsymbol{\phi},t),\ t) + \frac{\partial q_s(\boldsymbol{\phi},\ v_1(\boldsymbol{\phi},t),\ v_{gs}(\boldsymbol{\phi},t),\ v_{ds}(\boldsymbol{\phi},t),\ t)}{\partial t} \tag{24}$$

where i_{gc}, i_{dc} and i_{sc} represent the gate, drain and source conducting currents, respectively, q_g, q_d and q_s stand for the total charges on the gate, drain and source electrodes, respectively, and $\boldsymbol{\phi}$ is a parameter vector including, for instance, gate length, gate width, channel thickness, doping density, etc. According to (22)–(24), the model can be represented by the equivalent circuit shown in Fig. 5.

i_{gc}, i_{dc} and i_{sc} representing the gate, drain and source conducting currents in (22)–(24) can be obtained by integrating the current density $\boldsymbol{J}$ in (2) over the appropriate planes at y=0, x=L and x=0, respectively, as shown in Fig. 2. For example, the drain conducting current i_{dc} can be written in integral form as [148]

$$i_{dc} = \int \boldsymbol{J} \cdot d\boldsymbol{s} = -qW \int_0^a \mu(E(L,\ y))n(L,\ y)E_x(L,\ y)dy + qWD \int_0^a \nabla_x n(L,\ y)dy \tag{25}$$

where E_x and $\nabla_x n$ are the x components of $\boldsymbol{E}$ and ∇n, respectively, and W is the gate width.

The partial derivatives of the total charges q_g, q_d and q_s w.r.t. time t represent the displacement currents through the corresponding electrodes. q_g, q_d and q_s can be written in integral form [148]. For instance,

$$q_g = \varepsilon W \int_0^L E_y(x, 0)dx \tag{26}$$

where E_y is the y component of $\boldsymbol{E}$.

Since $\boldsymbol{E}(x, y)$ and $n(x, y)$ are dependent on the voltages v_1, v_{gs} and v_{ds}, the conducting currents and the total charges are nonlinear functions of v_1, v_{gs} and v_{ds}.

Under normal working conditions, the gate is reverse biased and the gate conducting current i_{gc} can be neglected. (The gate forward biasing and the drain breakdown conditions may be included by introducing diodes into the model [148].) With this assumption, the drain and source conducting currents are equal under DC conditions. In [142–144], the solution of v_1 is obtained iteratively until the difference between the drain and source conducting currents is small enough. In Section III, we discuss HB simulation where the spectrum of an output of interest is calculated iteratively. In order to avoid a double iteration loop and make the PBM computationally efficient, we combine v_1 with the HB iteration while satisfying the boundary conditions.

F. Performance Prediction and Parameter Extraction

One of the advantages of the PBMs over the ECMs is that the PBMs have better performance prediction capability. This capability gives device and circuit engineers an opportunity to preview the performance of the device and of the resulting circuit and improve their design if necessary.

Using the PBM described before we predict the DC performance of a MESFET used in [148]. The comparison of our result and Khatibzadeh's result [148] is shown in Fig. 6. Good agreement is observed though there are some discrepancies resulting from our modification of the original model [144].

For an ECM of FET, the intrinsic and extrinsic parameters are extracted from DC, small- and large-signal data [5-7, 149,150]. The accuracy and usefulness of the extracted model depends on the consistency of the application with measurements. It is obvious that ECMs are not traceable to device physical parameters.

PBM parameter extraction leads to physical parameters of the intrinsic device model, as well as linear elements of the extrinsic circuits. An advantage of PBMs is that it is relatively easy to estimate a good starting point for parameter extraction, since most of the model parameters should be physically meaningful and tangible. An important application of PBM parameter extraction is statistical modeling at the device physical and geometrical level, in which a large number of parameter extractions from a set of measured data is processed. This is discussed in Section IV.

Consider FET parameter extraction using our PBM. The schematic of the extrinsic and intrinsic model is shown in Fig. 7. The intrinsic parameters are defined in Table I. S-parameter measurements [151] in the frequency range 1GHz to 21GHz at 3 bias points (gate bias 0V, -0.84V, -1.54V and drain bias 5V) are processed simultaneously.

We used HarPE [128] for this parameter extraction. Measured values of gate length L, gate width W and doping density N_d are assigned as starting values. The efficient ℓ_1 optimizer [152] was selected. The parameter extraction process took approximately 6 CPU minutes and 22 iterations on a Sun SPARCstation 1. Optimizable extrinsic and intrinsic parameters before and after optimization are listed in Table II. A comparison between the measured S-parameters [151] and calculated S-parameters at the three bias points is shown in Fig. 8. Good agreement is obtained.

III. NONLINEAR CIRCUIT ANALYSIS

The responses of a nonlinear circuit can be determined by solving a set of state (differential) equations

$$f(\dot{\boldsymbol{x}},\ \boldsymbol{x},\ \boldsymbol{u},\ t) = \mathbf{0} \tag{27}$$

where $\boldsymbol{x} = [x_1\ x_2\ \ldots\ x_n]^T$ is a set of state variables, usually certain selected voltages or currents, and

$\boldsymbol{u} = [u_1\ u_2\ \ldots\ u_m]^T$ is the excitation vector. (27) can be solved in time-domain, frequency-domain, or mixed frequency/time-domain using respective methods.

In this section, we present nonlinear circuit analysis with PBMs of FETs using the HB method.

A. Formulation of the Harmonic Balance Equations

In this formulation the circuit is divided into a linear subcircuit, a nonlinear subcircuit and an excitation subcircuit as shown in Fig. 9. Assume the circuit has N nodes. Then the circuit equations in the time domain can be written as [50]

$$\boldsymbol{f}(\boldsymbol{v}(t),\ t) = \boldsymbol{i}(\boldsymbol{v}(t)) + \frac{d}{dt}\boldsymbol{q}(\boldsymbol{v}(t)) + \int_{-\infty}^{t} \boldsymbol{y}(t-\tau)\boldsymbol{v}(\tau)d\tau + \boldsymbol{i}_{ss}(t) = 0 \tag{28}$$

where t is time, $\boldsymbol{v}$ is a vector of node voltage waveforms, $\boldsymbol{i}_{ss}$ is the vector of source current waveforms from the excitation subcircuit, $\boldsymbol{i}$, $\boldsymbol{q}$ are differentiable vector functions representing the currents entering the nodes from the nonlinear resistors or nonlinear voltage controlled current sources, and the charges entering the nodes from the nonlinear capacitors, respectively, $\boldsymbol{y}$ is the matrix-valued impulse response of the linear subcircuit.

To use the HB technique, (28) is Fourier transformed into the frequency domain as [50]

$$\boldsymbol{F}(\boldsymbol{V}) = \boldsymbol{I}(\boldsymbol{V}) + j\boldsymbol{\Omega}\boldsymbol{Q}(\boldsymbol{V}) + \boldsymbol{Y}\boldsymbol{V} + \boldsymbol{I}_{ss} = 0 \tag{29}$$

where $\boldsymbol{V}$ is a vector that contains the Fourier coefficients of the voltage at each node and each harmonic, $\boldsymbol{Y}$ is a node admittance matrix for the linear subcircuit, $\boldsymbol{I}_{ss}$ contains the Fourier coefficients of the source current for each node and each harmonic, $\boldsymbol{I}$, $\boldsymbol{Q}$ correspond to the currents from the nonlinear resistors or nonlinear voltage controlled current sources and the charges from the nonlinear capacitors entering each node at each harmonic, respectively, and $\boldsymbol{\Omega}$ is the frequency matrix as defined in [50]. To accommodate Newton's method for solving the HB equation, (29) is reorganized into real equation form by splitting the real part and imaginary part of the complex numbers as

$$\overline{\boldsymbol{F}}(\overline{\boldsymbol{V}}) = \overline{\boldsymbol{I}}(\overline{\boldsymbol{V}}) + \overline{\boldsymbol{\Omega}}\,\overline{\boldsymbol{Q}}(\overline{\boldsymbol{V}}) + \overline{\boldsymbol{Y}\boldsymbol{V}} + \overline{\boldsymbol{I}}_{ss} = 0 \tag{30}$$

where a bar stands for a real vector resulting from the complex counterpart. For example,

$$\overline{\boldsymbol{V}} = \begin{bmatrix} Real(\boldsymbol{V}) \\ Imag(\boldsymbol{V}) \end{bmatrix}, \quad \overline{\boldsymbol{F}} = \begin{bmatrix} Real(\boldsymbol{F}) \\ Imag(\boldsymbol{F}) \end{bmatrix}$$

$\overline{\Omega}$ is a frequency matrix which can be written as

$$\overline{\Omega} = \begin{bmatrix} & & & & -\Omega(0) & & & \\ & & & & & -\Omega(\omega_1) & & \\ & & & & & & \cdots & \\ & & & & & & & -\Omega(\omega_H) \\ \Omega(0) & & & & & & & \\ & \Omega(\omega_1) & & & & & & \\ & & \cdots & & & & & \\ & & & \Omega(\omega_H) & & & & \end{bmatrix} \tag{31}$$

where $\Omega(\omega_i)$is a diagonal matrix whose diagonal elements are ω_i's. H is the number of harmonics used in the simulation.

B. Integration of Physics-based Model with HB Equation

The PBM of FET represented by (22)–(24) can be integrated into (30). The first problem in the simulation with the PBM is the calculation of the gate, drain and source currents. In order to determine the gate, drain and source currents, one must obtain the value of the intermediate parameter v_1 in (17). In the original approach [142–144], the condition $i_{dc} = i_{sc}$ was used to solve for v_1, neglecting the displacement currents. However, this condition is strictly valid at DC, but not for instantaneous currents under AC excitations. Also, a double iteration loop is required in the HB simulation. The first loop is devoted to solve for v_1 iteratively. The value of v_1 is then substituted into the second loop for solving the HB equations.

To make the simulation with the PBM computationally efficient, in our implementation we treat v_1 of (17b) as a state variable though it has no circuit interpretation. We integrate v_1 directly into the HB equations to allow it to vary w.r.t. time, RF input level, and operating frequencies [8], while satisfying the boundary conditions (17). To prove the validity of this integration, consider a nonlinear circuit with only one FET. Since we include v_1 in the state variable vector, we add the nodal equation at the node "Z", as indicated in Fig. 5, to the HB equation in order to uniquely solve for the state variable vector. Let

$$\boldsymbol{v}(\boldsymbol{\phi},\ t) = [v_1(\boldsymbol{\phi},\ t)\ v_{gs}(\boldsymbol{\phi},\ t)\ v_{ds}(\boldsymbol{\phi},\ t)]^T \tag{32}$$

$$\boldsymbol{i}(\boldsymbol{\phi},\ \boldsymbol{v}(\boldsymbol{\phi},\ t),\ t) = \boldsymbol{A} \begin{bmatrix} i_{gc}(\boldsymbol{\phi},\ \boldsymbol{v}(\boldsymbol{\phi},\ t),\ t) \\ i_{dc}(\boldsymbol{\phi},\ \boldsymbol{v}(\boldsymbol{\phi},\ t),\ t) \\ i_{sc}(\boldsymbol{\phi},\ \boldsymbol{v}(\boldsymbol{\phi},\ t),\ t) \end{bmatrix} \tag{33}$$

and

$$\boldsymbol{q}(\boldsymbol{\phi},\ \boldsymbol{v}(\boldsymbol{\phi},\ t),\ t) = \boldsymbol{B} \begin{bmatrix} q_g(\boldsymbol{\phi},\ \boldsymbol{v}(\boldsymbol{\phi},\ t),\ t) \\ q_d(\boldsymbol{\phi},\ \boldsymbol{v}(\boldsymbol{\phi},\ t),\ t) \\ q_s(\boldsymbol{\phi},\ \boldsymbol{v}(\boldsymbol{\phi},\ t),\ t) \end{bmatrix} \tag{34}$$

where $\boldsymbol{A}$ and $\boldsymbol{B}$ are simple incidence matrices containing 0's, 1's and −1's. Then, using the Fourier transformation and following (30), we can write the HB equation for a nonlinear circuit with a single FET as

$$\overline{\boldsymbol{F}}(\boldsymbol{\phi},\ \overline{\boldsymbol{V}}(\boldsymbol{\phi})) = \overline{\boldsymbol{I}}(\boldsymbol{\phi},\ \overline{\boldsymbol{V}}(\boldsymbol{\phi})) + \overline{\boldsymbol{\Omega}}\,\overline{\boldsymbol{Q}}(\boldsymbol{\phi},\ \overline{\boldsymbol{V}}(\boldsymbol{\phi})) + \overline{\boldsymbol{Y}}\,\overline{\boldsymbol{V}}(\boldsymbol{\phi}) + \overline{\boldsymbol{I}}_{ss} = \boldsymbol{0} \tag{35}$$

where the admittance matrix $\overline{\boldsymbol{Y}}$ is modified to include the pseudo-node "Z" which is isolated from the linear part of the circuit. Because of the introduction of the pseudo-node, (35) automatically ensures current continuity at all harmonics, i.e.,

$$\overline{\boldsymbol{I}}_g + \overline{\boldsymbol{I}}_d + \overline{\boldsymbol{I}}_s = \boldsymbol{0} \tag{36}$$

This in turn, ensures current continuity in the time domain

$$i_g(t) + i_d(t) + i_s(t) = 0 \tag{37}$$

Therefore, our condition is valid not only for DC but also for small- and large-signal RF operations.

C. Solution of the HB Equation

The Newton update for solving the HB equation can be written as

$$\overline{\boldsymbol{V}}_{new}(\boldsymbol{\phi}) = \overline{\boldsymbol{V}}_{old}(\boldsymbol{\phi}) - \left[\overline{\boldsymbol{J}}(\boldsymbol{\phi},\ \overline{\boldsymbol{V}}_{old}(\boldsymbol{\phi}))\right]^{-1}\overline{\boldsymbol{F}}(\boldsymbol{\phi},\ \overline{\boldsymbol{V}}_{old}(\boldsymbol{\phi})) \tag{38}$$

where $\overline{J}(\phi, \overline{V}(\phi))$ is the Jacobian matrix used in the algorithm. From (35), we obtain the Jacobian as

$$\overline{J}(\phi, \overline{V}(\phi)) = \left[\frac{\partial \overline{I}^T(\phi, \overline{V}(\phi))}{\partial \overline{V}(\phi)} \right]^T + \overline{\Omega} \left[\frac{\partial \overline{Q}^T(\phi, \overline{V}(\phi))}{\partial \overline{V}(\phi)} \right]^T + \overline{Y} . \tag{39}$$

Note that in solving the HB equation, ϕ is constant and $\overline{V}(\phi)$ is variable. Following [50], in order to calculate the entries of $\overline{J}(\phi, \overline{V}(\phi))$, we must first obtain the derivatives of i and q w.r.t. v. Since v_1 is considered as a state variable, the entries of $\overline{J}(\phi, \overline{V}(\phi))$ include the derivatives of $\overline{I}$ and $\overline{Q}$ w.r.t. $\overline{V}_1$. For instance, let $\overline{I}_{dc}(\phi, \overline{V}(\phi), \omega_k)$ represent the split real and imaginary parts of the kth harmonic component of the drain conducting current and $\overline{V}_1(\phi, \omega_l)$ represent the split real and imaginary parts of the lth harmonic component of variable v_1, then

$$\frac{\partial \overline{I}_{dc}^T(\phi, \overline{V}(\phi), \omega_k)}{\partial \overline{V}_1(\phi, \omega_l)} = \begin{bmatrix} G_{v_1}^R(\omega_{k-l}) + G_{v_1}^R(\omega_{k+l}) & G_{v_1}^I(\omega_{k+l}) - G_{v_1}^I(\omega_{k-l}) \\ G_{v_1}^I(\omega_{k-l}) + G_{v_1}^I(\omega_{k+l}) & G_{v_1}^R(\omega_{k-l}) - G_{v_1}^R(\omega_{k+l}) \end{bmatrix}^T \tag{40}$$

where

$$G_{v_1}^R(\omega_i) \triangleq \frac{1}{T_0} \int_0^{T_0} \frac{\partial i_{dc}(\phi, v(\phi), t)}{\partial v_1(\phi, t)} \cos(\omega_i t) dt \tag{41a}$$

$$G_{v_1}^I(\omega_i) \triangleq -\frac{1}{T_0} \int_0^{T_0} \frac{\partial i_{dc}(\phi, v(\phi), t)}{\partial v_1(\phi, t)} \sin(\omega_i t) dt \tag{41b}$$

and ω_i is the ith harmonic frequency. T_0 is the period of the waveform. The derivatives of i and q w.r.t. v are evaluated by differentiating the corresponding terms of (22)–(24) w.r.t. v. For example, differentiating (25) w.r.t. v_1 gives

$$\frac{\partial i_{dc}}{\partial v_1} = -qW \int_0^a \left[\frac{\partial \mu}{\partial E}\frac{\partial E}{\partial v_1} n E_x + \mu \frac{\partial n}{\partial v_1} E_x + \mu n \frac{\partial E_x}{\partial v_1} \right]_{x=L} dy + qWD \int_0^a \left[\frac{\partial (\nabla_x n)}{\partial v_1} \right]_{x=L} dy \quad (42)$$

though in our actual implementation the perturbation technique is used to avoid these complicated analytical formulations. When the derivatives of $\boldsymbol{i}$ and $\boldsymbol{q}$ w.r.t. $\boldsymbol{v}$ are obtained, the entries of the Jacobian matrix $\overline{\boldsymbol{J}}$ can be evaluated by the Fourier transform. We discuss in Section IV that at the solution of the HB equation $\overline{\boldsymbol{J}}$ can be reused in adjoint analysis for design optimization.

IV. GRADIENT-BASED OPTIMIZATION

Circuit design using ECMs has been extensively studied. Little work has been devoted to design optimization using PBMs. Here, we present a novel approach to integrated PBM, HB, gradient-based optimization.

A. Sensitivity Analysis

The most popular sensitivity analysis method is the conventional *P*erturbation *A*pproximation *S*ensitivity *T*echnique (*PAST*). In this method, the first-order derivative of $f(\boldsymbol{\phi})$ w.r.t. ϕ_i is estimated by

$$\frac{\partial f(\boldsymbol{\phi})}{\partial \phi_i} = \frac{f(\boldsymbol{\phi} + \Delta\phi_i \boldsymbol{u}_i) - f(\boldsymbol{\phi})}{\Delta\phi_i} \quad (43)$$

where $\Delta\phi_i \boldsymbol{u}_i$ denotes the perturbation of the ith variable, $\Delta\phi_i$ is the perturbation length and $\boldsymbol{u}_i$ is a unit vector which has 1 in the ith position and zeros elsewhere. This method is straightforward and easy to implement though it may not be accurate enough. However, the computational effort involved grows in proportion to the dimension of the problem. It can be extremely inefficient for large-scale problems.

Bandler, Chen, Daijavad and Madsen [153] proposed an *I*ntegrated *G*radient *A*pproximation *T*echnique (*IGAT*) which incorporates the use of perturbations, the Broyden update [154]

$$\nabla f(\boldsymbol{\phi}_{new}) = \nabla f(\boldsymbol{\phi}_{old}) + \frac{f(\boldsymbol{\phi}_{new}) - f(\boldsymbol{\phi}_{old}) - (\nabla f(\boldsymbol{\phi}_{old}))^T \Delta\boldsymbol{\phi}}{\Delta\boldsymbol{\phi}^T \Delta\boldsymbol{\phi}} \Delta\boldsymbol{\phi} \ . \tag{44}$$

and the special iteration of Powell [155]. Perturbations with (43) are used to obtain an initial approximation as well as regular corrections. $\boldsymbol{\phi}_{old}$ and $\boldsymbol{\phi}_{new}$ are two different points and $\Delta\boldsymbol{\phi} = \boldsymbol{\phi}_{new} - \boldsymbol{\phi}_{old}$. *IGAT* is robust and has been applied to microwave circuit design [153] and yield optimization [63].

Efficient and accurate sensitivity analysis for HB can be achieved by the *E*xact *A*djoint *S*ensitivity *T*echnique (*EAST*) developed by Bandler, Zhang and Biernacki [156], which is a generalization of the linear adjoint sensitivity analysis technique. For example, the sensitivity of an output voltage V_{out} w.r.t. a parameter ϕ_i of a nonlinear element at branch b can be expressed by

$$\frac{\partial \overline{V}_{out}}{\partial \phi_i} = \begin{cases} -\sum_k Real\left[\hat{V}_b(k) G_b^*(k)\right] & \text{if } \phi_i \in \text{nonlinear current sources} \\ -\sum_k Imag\left[\hat{V}_b(k) G_b^*(k)\right] & \text{if } \phi_i \in \text{nonlinear capacitors} \end{cases} \tag{45}$$

where the complex quantity $\hat{V}_b(k)$ is the voltage of branch b at harmonic k and is obtained from an adjoint network analysis. $G_b(k)$ denotes the sensitivity expression of the element containing variable ϕ_i [156]. * stands for the conjugate of a complex number. The efficiency of *EAST* has been demonstrated in a nonlinear parameter extraction program [7]. This technique enjoys high computational efficiency but suffers from implementation difficulties.

To exploit the efficiency of *EAST* and simplicity of *PAST*, Bandler *et al.* proposed the *F*easible *A*djoint *S*ensitivity *T*echnique (*FAST*) [157]. It features high speed gradient computation as well as easy implementation. It is particularly suitable for general purpose CAD programs. We choose *FAST* here for the integration of efficient gradient-based optimization with PBMs.

B. Integration of FAST with Physics-Based Models

Consider the circuit responses be represented by

$$R(\phi) = \Re(\phi, \overline{V}(\phi)), \tag{46}$$

which may include output voltage, current, power, power gain, etc. Let S be a set of design specifications. Then the objective function for a design problem can be expressed as

$$U(\phi) = U(R(\phi), S) \tag{47}$$

and the corresponding optimization as

$$\underset{\phi}{minimize} \quad U(\phi) \ . \tag{48}$$

In order to solve (48), the derivatives of U w.r.t. each variable ϕ_i in ϕ need to be calculated. Let ϕ_i be a generic design variable such as a device dimension or doping density. The sensitivity of U w.r.t. ϕ_i can be obtained by differentiating (47) w.r.t. ϕ_i

$$\frac{\partial U}{\partial \phi_i} = \left[\frac{\partial U}{\partial R} \right]^T \frac{\partial R}{\partial \phi_i} \ . \tag{49}$$

$\frac{\partial U}{\partial R}$ depends on the form of the objective function. $\frac{\partial R}{\partial \phi_i}$ can be derived from (46)

$$\frac{\partial R(\phi)}{\partial \phi_i} = \frac{\partial \Re(\phi, \overline{V}(\phi))}{\partial \phi_i} + \left[\frac{\partial \Re^T(\phi, \overline{V}(\phi))}{\partial \overline{V}(\phi)} \right]^T \frac{\partial \overline{V}(\phi)}{\partial \phi_i} \tag{50}$$

where $\frac{\partial \Re}{\partial \phi_i}$ and $\frac{\partial \Re^T}{\partial \overline{V}}$ may be calculated analytically or by perturbation. The *FAST* technique is applied to calculate $\frac{\partial \overline{V}}{\partial \phi_i}$.

Assume that the solution of the HB equation is $\overline{V} = \overline{V}_{solution}$, i.e.,

$$\overline{F}(\phi, \overline{V}_{solution}) = 0 \ . \tag{51}$$

The *FAST* technique proceeds by obtaining

$$\overline{e}^T \frac{\partial \overline{V}(\phi)}{\partial \phi_i} = - \hat{\overline{V}}^T \frac{\overline{F}(\phi + \Delta\phi_i u_i, \overline{V}_{solution})}{\Delta \phi_i} \tag{52}$$

where $\overline{e}$ is a vector containing 1's and 0's and is used to select the real and imaginary parts of a complex output of interest. The adjoint voltage $\hat{\overline{V}}$ is the solution of the adjoint system

$$[\overline{J}(\phi,\ \overline{V}(\phi))]^T \hat{\overline{V}} = \overline{e} \tag{53}$$

where $\overline{J}(\phi,\overline{V}(\phi))$ is the Jacobian matrix defined by (39). It is typically available in the form of LU factors at the solution of the HB equation.

As an example, consider the sensitivity of an output voltage w.r.t. the gate width W of a FET, i.e. $\overline{e}^T \frac{\partial \overline{V}(\phi)}{\partial W}$. We need to obtain the adjoint solution $\hat{\overline{V}}$ and evaluate the HB residual function $\overline{F}(W+\Delta W,\ \overline{V}_{solution})$. By reusing the Jacobian matrix available at the HB solution, the adjoint system can be solved with relatively little additional effort. The HB residual function is evaluated from (35) as

$$\overline{F}(W+\Delta W,\ \overline{V}_{solution}) = \overline{I}(W+\Delta W,\ \overline{V}_{solution}) + \overline{\Omega}\overline{Q}(W+\Delta W,\ \overline{V}_{solution}) + \overline{Y}\ \overline{V}_{solution} + \overline{I}_{ss}\ . \tag{54}$$

Note that $\overline{V}_{solution}$ is constant at this stage and there is no iteration involved. For instance, the value of i_{dc} can be calculated by replacing W by $W+\Delta W$ in (25), where E and n are evaluated at the voltage solution $v_{solution}$ obtained by the inverse Fourier transform of $\overline{V}_{solution}$. The resulting i_{dc} is then transformed to the frequency domain to be used in (54). This provides high speed yet simple gradient evaluation for gradient optimizers.

C. Algorithm for Optimization

Step 1 Initialization for Optimization

Step 1.1 Input the circuit topology and design specifications.

Step 1.2 Initialize the parameter vector ϕ. Assign values to all parameters in the circuit including the physical parameters and parasitic parameters of the FETs.

Step 2 Time Domain Simulation

Step 2.1 Initialize $\overline{V}(\phi)$.

Step 2.2 Convert $\overline{V}(\phi)$ to $v(\phi,\ t)$, i.e., v_1, v_{gs} and v_{ds}, using the inverse Fourier transform. Calculate the gate, drain and source conducting current $i(\phi,\ v(\phi,\ t),\ t)$ and gate, drain and source total charge $q(\phi,\ v(\phi,\ t),\ t)$.

Step 3 Frequency Domain Simulation

Step 3.1 Use the forward Fourier transform to obtain $\overline{I}(\phi, \overline{V}(\phi))$ and $\overline{Q}(\phi, \overline{V}(\phi))$ from $i(\phi, v(\phi, t), t)$ and $q(\phi, v(\phi, t), t)$.

Step 3.2 Solve the HB equation using the Newton update (38). Note that at this stage ϕ is constant and $\overline{V}(\phi)$ is variable. If $\overline{V}(\phi)$ is the solution of HB equation $\overline{F}(\phi, \overline{V}(\phi)) = 0$, then go to *Step 4*. Otherwise, update $\overline{V}(\phi)$. Go to *Step 2.2*.

Step 4 Optimization of Parameter ϕ

Step 4.1 If ϕ is optimal, stop.

Step 4.2 Solve the adjoint system (53) using the Jacobian matrix available at the solution of the HB equation. Calculate $\frac{\partial \overline{V}(\phi)}{\partial \phi_i}$ using (52). Evaluate $\frac{\partial R(\phi)}{\partial \phi_i}$ using (50) and then $\frac{\partial U(\phi)}{\partial \phi_i}$ using (49), for $i = 1, 2, ..., M$, where M is the number of optimizable parameters.

Step 4.3 Update ϕ according to the optimization algorithm. Go to *Step 2*.

This algorithm is illustrated by the flowchart in Fig. 10.

V. STATISTICAL MODELING

Due to the deviations of device parameters in manufacturing, device performance varies according to the parameter distributions. Statistical modeling is used to model the statistical characteristics of the devices and to provide accurate models for yield-driven design. In this section we discuss statistical modeling of FETs with PBMs. Basic definitions and formulas such as mean value, standard deviation and correlation coefficient are provided in the Appendix.

A. Parameter Extraction and Statistical Estimation

Statistical modeling requires measurements on a large sample of devices. The measurements may include DC, small-signal and large-signal data. For each device, a set of model parameters is extracted from the corresponding measurements, providing a sample of models. The statistical model is based on the resulting sample of models. It is essential for the success of such an approach to have

a parameter extraction procedure which produces efficient, consistent and unique solutions.

Suppose we have a set of data with m measurements

$$\boldsymbol{S}^i = [S_1^i \; S_2^i \; \ldots \; S_m^i]^T \tag{55}$$

corresponding to the ith device, $i = 1, 2, \ldots, K$, and K is the total number of devices measured. Let

$$\boldsymbol{\phi}^i = [\phi_1^i \; \phi_2^i \; \ldots \; \phi_n^i]^T \tag{56}$$

be the model parameters of the ith device. Assume the device responses corresponding to the measurement $\boldsymbol{S}^i$ to be

$$\boldsymbol{R}(\boldsymbol{\phi}^i) = [R_1(\boldsymbol{\phi}^i) \; R_2(\boldsymbol{\phi}^i) \; \ldots \; R_m(\boldsymbol{\phi}^i)]^T \; . \tag{57}$$

The parameter extraction problem can be formulated as

$$\min_{\boldsymbol{\phi}^i} \sum_{j=1}^{m} w_j^i \, | R_j(\boldsymbol{\phi}^i) - S_j^i |^p \qquad 1 \le p \tag{58}$$

where w_j^i is a weighting factor and p=1 or 2 results in ℓ_1 or ℓ_2 (least squares) optimization. The optimization is performed for each device measured, i.e., for $i = 1, 2, \ldots, K$.

The statistics of the model parameters are estimated by mean values ν, standard deviations σ and correlation coefficients r between different model parameters after statistical parameter extraction. The estimated statistical parameters ν, σ and r are usually sufficient to represent the multidimensional normal distribution. For an arbitrary distribution, the discretized probability density function (PDF) based on the available data can be used to approximate the joint PDF [74,158].

B. Hierarchical Statistical Modeling

A statistical model can be described by ν, σ and r of a statistical distribution at the device response level, the equivalent circuit model parameter level and/or the basic physical parameter level as shown in Fig. 11. We can create the statistical model based on ECMs or PBMs from statistical outcomes of the device via parameter extraction. Statistical models from PBMs can also be determined directly from the statistical information on the physical parameters. The models, in turn,

can be used to generate simulated statistical outcomes of the device.

ECM statistical modeling leads to the statistical distributions of the equivalent circuit parameters [73,84]. The advantage of this approach is that equivalent circuit models are usually available in popular microwave CAD software and model evaluation is quite efficient. However, there are serious limitations in such an approach. It is difficult to relate the statistical distributions of ECM parameters to those of the device physical parameters. Statistical variations in a single physical parameter may affect many ECM parameters, and at the same time each ECM parameter may be affected by many physical parameters. Consequently, the equivalent circuit model parameters are correlated and such correlations are difficult to estimate. Furthermore, this nonlinear mapping may result in complicated and non-Gaussian distributions.

In a recent paper by Bandler *et al.* [86] statistical modeling of a GaAs MESFET by the Materka ECM [3] was investigated. Even though for individual device models the fit of the ECM model responses to the measurements are excellent, the statistical model extracted from the ECM sample including mean value, standard deviation, correlations, etc., failed to satisfactorily reproduce the original measurement statistics.

Statistical modeling using PBMs leads to the statistical distributions of the device physical parameters [86]. The statistical distributions at this level are simpler than those at the equivalent circuit level. A smaller number of statistically independent variables can be used. Since we are directly dealing with statistical perturbations at the lowest level, the assumption of a normal distribution may be justified. Also, with PBMs it is much easier to identify both the parameters that are subject to significant statistical variations and the parameters which are correlated. Therefore, PBM statistical modeling should be more accurate and reliable. This is probably the most appropriate approach to statistical modeling. The disadvantage of this method is that the model evaluation may be much slower than that of the ECMs.

C. Physics-Based Statistical Modeling

As an example, we use the Ladbrooke model [159] and the Khatibzadeh and Trew model [144]

to illustrate PBM statistical modeling.

The Ladbrooke model uses a small-signal equivalent circuit whose components are derived from the physical parameters and the bias conditions, i.e., the model is defined in terms of device physical parameters. The equivalent circuit of the Ladbrooke model is shown in Fig. 12. g_m, τ, r_0, C_{gs}, C_{dg}, R_i, R_d, R_s, and L_g are functions of the physical parameters and bias conditions. For example [159],

$$g_m = \frac{\varepsilon v_s W}{d} \tag{59}$$

$$C_{gd} = \frac{2\varepsilon W}{1 + \frac{2X}{L}} \tag{60}$$

$$L_g = \frac{\mu_0 d W}{m^2 L} + L_{g0} \tag{61}$$

where ε is the permittivity of GaAs, v_s the saturation electron drift velocity, W the gate width, L the gate length, μ_0 the permeability of free space, m the number of gate fingers, and L_{g0} is introduced to include the inductances from gate bond wires and pads. d is the equivalent depletion depth which is defined as

$$d = \sqrt{2\varepsilon \frac{V_{B0} - V_{G'S'}}{qN_d}} \tag{62}$$

and X is the voltage dependent space-charge layer extension defined as

$$X = a_0(V_{D'G'} + V_{B0}) \sqrt{\frac{2\varepsilon}{qN_d(V_{B0} - V_{G'S'})}} \tag{63}$$

where V_{B0} is the zero-bias barrier potential and a_0 is a proportionality coefficient. The drain output resistor r_0 is approximated by [86]

$$r_0 = r_{01} V_{D'S'}(r_{03} - V_{G'S'}) + r_{02} \tag{64}$$

where r_{01}, r_{02} and r_{03} are the parameters to be determined, $V_{G'S'}$, $V_{D'G'}$ and $V_{D'S'}$ are the intrinsic

gate-to-source, drain-to-gate and drain-to-source voltages, respectively (see Fig. 12). The rest of the elements of the equivalent circuit, R_g, L_d, L_s, G_{ds} and C_{ds}, are assumed to be linear components. We keep the gate width W fixed. Therefore, the model parameters to be extracted are

$$\{L, a, N_d, v_s, V_{B0}, a_0, r_{01}, r_{02}, r_{03}, L_{g0}, R_g, L_d, L_s, G_{ds}, C_{ds}\}$$

where a is the channel thickness.

The parameters of the Khatibzadeh and Trew model are listed in Table I.

Statistical modeling was performed on a sample of GaAs MESFET measurements provided by Plessey Research Caswell [151]. 69 individual devices (data sets) from two wafers were used. Each device represents a four finger 0.5μm gate length GaAs MESFET with equal finger width of 75μm. Each data set contains small-signal S-parameters measured under three different bias conditions and at frequencies from 1GHz to 21GHz with a 0.4GHz step. DC drain bias current is also included in the measurements.

HarPE [128] was used to carry out statistical modeling. We first performed parameter extraction for each individual device by matching simultaneously the DC and small-signal S-parameter responses to the corresponding measurements [6]. The resulting sample of 69 models was postprocessed to obtain the mean values of the parameters. The same procedure was repeated once more using the mean values as new initial parameter values. After parameter extraction, the resulting samples were then postprocessed to obtain the parameter statistics, including the mean value, standard deviation and the discrete distribution function (DDF) [84] for each parameter, as well as the correlations between the parameters.

The parameter mean values and standard deviations of the Ladbrooke model and those of the Khatibzadeh and Trew model are listed in Table III. The histograms of the FET gate length L and doping density N_d for both models are illustrated in Figs. 13 and 14, respectively. We notice from Table III that there are discrepancies in certain common parameters between the two models. Those differences may result from different approximations and different model structures adopted by the two models. The standard deviations of the parameters of the Khatibzadeh and Trew model are

noticeably smaller than those of the Ladbrooke model. We are not satisfied with the results. Further investigation is planned.

The two statistical models created by postprocessing were examined using Monte Carlo simulations. The statistical characteristics of the S-parameters generated by the statistical models were compared with the measurements. The comparison was made at bias point V_{GS} = 0V and V_{DS} = 5V and at frequency 11GHz. The Monte Carlo simulation was performed with 400 outcomes from the mean values, standard deviations, correlations and DDFs of the model parameters. The mean values and standard deviations of the measured and the simulated S-parameters from the Ladbrooke model and from the Khatibzadeh and Trew model are listed in Table IV. The histograms of one S-parameter are plotted in Fig. 15.

The standard deviation fits of the S-parameters from the measurement and the Ladbrooke model are quite good, as shown in Table IV [86]. The mean values from the Ladbrooke model do not fit the measurement well, which may indicate that the model is not flexible enough. The mean value match by the Khatibzadeh and Trew model is better than that by the Ladbrooke model. However, the standard deviations of the S-parameters from the Khatibzadeh and Trew model are smaller than those from the measurement except for $|S_{21}|$. This is consistent with the observation that the parameter standard deviations of the Khatibzadeh and Trew model are very small in Table III.

The postprocessed statistical model can be used for both nominal and Monte Carlo simulations. In nominal simulation, the parameters assume their mean values. In Monte Carlo simulation, statistical outcomes are generated from the parameter statistics. The most important application of statistical models is for statistical design or yield optimization.

VI. YIELD OPTIMIZATION OF MMICs

In the production of MMICs, devices are designed and manufactured in batches rather than individually. Random variations in the manufacturing process typically result in some failed devices which do not meet design specifications. Yield optimization, which takes into account the

manufacturing tolerances, model uncertainties, variations of process parameters and environmental uncertainties, etc., has become an important tool to reduce the cost of manufacturing.

In this section, we present yield optimization of MMICs with PBMs. As design variables we directly consider physical parameters for both active and passive devices. The parameters may include, for example, FET gate length, gate width, doping density, the number of turns of spiral inductors, geometry dimensions of metal–insulator–metal (MIM) capacitors, etc. The statistics of the parameters are modeled by a multidimensional normal distribution. Statistical correlations between parameters are also considered, which is very important for MMICs. The efficient *FAST* sensitivity technique is employed to permit high speed gradient-based yield optimization.

A. Formulation of Yield Optimization Problem

Assume that there are M failed devices out of N total outcomes. The production yield is simply defined as

$$Y = 1 - \frac{M}{N} \tag{65}$$

Let the parameters of a nominal circuit design be $\boldsymbol{\phi}^0$. The manufactured outcomes $\boldsymbol{\phi}^i$, $i = 1, 2, ..., N$, are spread around $\boldsymbol{\phi}^0$ according to the statistical distributions of the parameters and can be represented by

$$\boldsymbol{\phi}^i = \boldsymbol{\phi}^0 + \Delta\boldsymbol{\phi}^i \tag{66}$$

Corresponding to the jth design specification S_j, $j = 1, 2, ..., m$, the error function is defined as

$$e_j(\boldsymbol{\phi}^i) = R_j(\boldsymbol{\phi}^i) - S_j \tag{67a}$$

if S_j is an upper specification, or as

$$e_j(\boldsymbol{\phi}^i) = S_j - R_j(\boldsymbol{\phi}^i) \tag{67b}$$

if S_j is a lower specification.

Let

$$e(\phi^i) = [e_1(\phi^i)\ e_2(\phi^i)\ \ldots\ e_m(\phi)]^T \tag{68}$$

If all the entries of $e(\phi^i)$ are nonpositive, the outcome ϕ^i is acceptable. From (68) we create the generalized l_p function $p(\phi^i)$ as

$$v(\phi^i) = \begin{cases} \left[\sum_{j \in J(\phi^i)} [e_j(\phi^i)]^p \right]^{1/p} & \text{if } J(\phi^i) \neq \varnothing \\ -\left[\sum_{j=1}^{m} [-e_j(\phi^i)]^{-p} \right]^{-1/p} & \text{if } J(\phi^i) = \varnothing \end{cases} \tag{69}$$

where

$$J(\phi^i) = \{\, j \mid e_j(\phi^i) \geq 0 \,\} \tag{70}$$

The one-sided l_1 objective function for yield optimization [72] can be formulated as

$$U(\phi^0) = \sum_{i \in I} \alpha_i\ v(\phi^i) \tag{71}$$

where

$$I = \{\, i \mid v(\phi^i) > 0 \,\} \tag{72}$$

and α_i are positive multipliers. If we choose α_i as [72]

$$\alpha_i = \frac{1}{|\ v(\phi^i)\ |}\ , \tag{73}$$

the value of function $U(\phi^0)$ would be equal to M and the yield would be

$$Y(\phi^0) = 1 - \frac{U(\phi^0)}{N}\ . \tag{74}$$

Hence, the relation between yield and error functions is created and the maximization of yield is converted to the minimization of $U(\phi^0)$, i.e.,

$$\underset{\phi^0}{\text{minimize}} \quad U(\phi^0) \tag{75}$$

In our implementation α_i are assigned according to (73) at the starting point and fixed during

the optimization. With this process $U(\phi^0)$ will not be equal to M during optimization, but it provides a continuous approximation function to M [72].

B. Physics-Based Models for MMIC Active and Passive Devices

We use the PBM described in Section II to model GaAs MESFETs. Passive devices can be represented in general by their n-port Y matrices. For two terminal components, the two-port Y matrix is

$$\begin{bmatrix} I_1 \\ I_2 \end{bmatrix} = \begin{bmatrix} Y_{11}(\phi) & Y_{12}(\phi) \\ Y_{21}(\phi) & Y_{22}(\phi) \end{bmatrix} \begin{bmatrix} V_1 \\ V_2 \end{bmatrix} \tag{76}$$

where ϕ stands for physical parameters. For example, for MIM capacitors ϕ includes the geometrical dimensions of the metal plate, the dielectric constant and the thickness of the dielectric film. For spiral inductors, ϕ includes the substrate height, the conductor width and spacing, and the number of turns. The configuration and schematics of spiral inductors, MIM capacitors and planar resistors are shown in Fig. 16.

From the equivalent circuits of the passive devices we can calculate the corresponding Y matrices. The elements of the equivalent circuits are derived from the physical parameters ϕ. The passive device models are, therefore, defined in terms of physical parameters. For instance, the value of capacitance C in the equivalent circuit for an MIM capacitor can be evaluated by [160]

$$C = \frac{10^{-3}\varepsilon_{rd} w l}{36\pi d} \tag{77}$$

where C is in pF, ε_{rd} is the relative permittivity of the dielectric film, w and l are the width and length of the metal plate in μm, respectively, and d is the thickness of the dielectric film in μm.

With PBMs of the active and passive devices, we can directly use the physical parameters as design variables to perform yield optimization of MMICs.

C. Quadratic Approximation of Responses and Gradients

Yield optimization requires substantial computational effort for circuit simulations and, if gradient optimization is used, for gradient evaluations. Quadratic approximation is an efficient

approach to speed up the optimization process [118,161,162].

The circuit response $R(\boldsymbol{\phi})$ can be approximated by a quadratic model of the form

$$R(\boldsymbol{\phi}) = a_0 + \sum_{i=1}^{n} a_i(\phi_i - r_i) + \sum_{\substack{j,i=1 \\ j \geq i}}^{n} b_{ij}(\phi_i - r_i)(\phi_j - r_j) \tag{78}$$

where

$$\boldsymbol{r} = [r_1 \; r_2 \; \ldots \; r_n]^T \tag{79}$$

is a known reference point and

$$\boldsymbol{a} = [a_0 \; a_1 \; \ldots \; a_n]^T \tag{80a}$$

$$\boldsymbol{b} = [b_{11} \; b_{22} \; \ldots \; b_{nn} \; b_{12} \; b_{13} \; \ldots \; b_{n-1,n}]^T \tag{80b}$$

are the quadratic model parameters to be determined. According to [118,162], $\boldsymbol{a}$ and $\boldsymbol{b}$ can be determined by using k, $n+1 \leq k \leq 2n+1$, function values calculated at k predetermined base points.

The gradient of $R(\boldsymbol{\phi})$ is a vector of functions, each function being the partial derivative of $R(\boldsymbol{\phi})$ w.r.t. one designable variable. In yield optimization we typically deal with four types of variables, namely, n_{DS} designable variables $\boldsymbol{\phi}_{DS}$ with statistics, n_D designable variables $\boldsymbol{\phi}_D$ without statistics, n_{FS} non-designable variables $\boldsymbol{\phi}_{FS}$ with statistical variations, and n_F non-designable parameters $\boldsymbol{\phi}_F$ without statistical variations. The gradients of $R(\boldsymbol{\phi})$ with respect to the designable variables can be written as

$$\nabla R = \left[\left(\frac{\partial R}{\partial \boldsymbol{\phi}_{DS}^0} \right)^T \quad \left(\frac{\partial R}{\partial \boldsymbol{\phi}_D^0} \right)^T \right]^T \tag{81}$$

The dimension of ∇R is $(n_{DS}+n_D)$. Each element in ∇R can be approximated by the quadratic model (78).

For yield optimization we need to calculate all the responses of interest and their gradients at a number of statistical outcomes. Each statistical outcome is generated in a $(n_{DS}+n_{FS})$-dimensional

space according to the corresponding distributions of the statistical variables ϕ_{DS} and ϕ_{FS}. Following (66), the statistical variables can be expressed as

$$\phi_S = [\phi_{DS}^T \; \phi_{FS}^T]^T = [(\phi_{DS}^0)^T \; (\phi_{FS}^0)^T]^T + [(\Delta\phi_{DS})^T \; (\Delta\phi_{FS})^T]^T \tag{82}$$

In order to save computational effort, we can build the circuit response models in the $(n_{DS}+n_{FS})$-dimensional space using ϕ_S as the variables in the quadratic model (78).

The quadratic models for responses as well as gradients are built for the current (optimization specific) nominal point and utilized for as many statistical outcomes as desired.

D. FAST Gradient Based Yield Optimization with Statistical Models

Gradient based yield optimization involves repeated simulation of a large number of statistical outcomes and requires sensitivity analysis to estimate the gradients of error functions. Therefore, an effective and efficient approach to gradient calculation is very important. Two gradient estimation techniques *IGAT* and *FAST*, as discussed in Section IV, have been used in yield optimization of nonlinear circuits [63]. We use *FAST* here for physics-based yield optimization.

In order to solve the yield optimization problem (75), we need to calculate the gradients of the objective function U w.r.t. the design variables. Let ϕ_k^0 be a generic design variable out of ϕ^0. Differentiating (69) w.r.t. ϕ_k^0 we obtain, if $J(\phi^i) \neq \varnothing$,

$$\frac{\partial v(\phi^i)}{\partial \phi_k^0} = \left(\sum_{j \in J(\phi^i)} [e_j(\phi^i)]^p \right)^{\frac{1}{p}-1} \sum_{j \in J(\phi^i)} [e_j(\phi^i)]^{p-1} \left[\frac{\partial e_j(\phi^i)}{\partial \phi^i} \right]^T \frac{\partial \phi^i}{\partial \phi_k^0} \tag{83}$$

$\frac{\partial \phi^i}{\partial \phi_k^0}$ can be evaluated through the relationship between ϕ^i and ϕ^0 in (66). The computation of $\frac{\partial e_j(\phi^i)}{\partial \phi^i}$ can be converted to the calculation of the gradients of circuit responses, i.e., we can express the gradient of $e_j(\phi^i)$ w.r.t. the lth element ϕ_l^i in ϕ^i as, from (67a) and (67b)

$$\frac{\partial e_j(\phi^i)}{\partial \phi_l^i} = \pm \frac{\partial R_j(\phi^i)}{\partial \phi_l^i} \tag{84}$$

where the sign depends on the type of the specification S_j. If S_j is an upper (lower) specification, the positive (negative) sign is used. The *FAST* technique can be used to evaluate $\frac{\partial R_j(\phi^i)}{\partial \phi_k^i}$ which provides efficient gradient calculation for yield optimization.

Since yield optimization deals with a number of statistical outcomes, an appropriate statistical device model is required for generating these outcomes. By using PBM statistical models described in Section V, yield optimization can be performed directly with the physical, geometrical and process-related parameters. The yield optimization at this level becomes more meaningful and practical than that at the equivalent circuit level, especially for yield-driven design of MMICs.

E. Yield Optimization of A Three Stage X-band MMIC Amplifier

We consider a three stage small-signal X-band cascadable MMIC amplifier shown in Fig. 17. The design is based on the circuit topology and the fabrication layout described in [163], but with different parameter values. The amplifier contains three MESFETs using an interdigitated structure with two gate fingers of dimensions 200μm×1.0μm. The matching circuits are composed of inductors and capacitors arranged in bandpass topology. All passive components are realized using lumped MMIC elements: spiral inductors, MIM capacitors and bulk resistors. The second and third MESFET are biased through a 1500Ω GaAs bulk resistor. The drains and the first gate bias are bypassed by a high value MIM capacitor. The input-output matching circuit includes a series capacitor to make the amplifier cascadable without additional components.

The amplifier is to meet the following specifications. In the passband (8GHz - 12GHz) gain = 14±2dB and VSWR < 2. In the stopband (below 6GHz or above 15GHz) gain < 2dB.

First, a nominal design is performed using minimax optimization [164], where the PBMs for the MESFETs and equivalent circuit models for all passive elements are used. As in a traditional design, only the matching circuits are optimized. The parameters of the active devices (MESFETs) have fixed values. There are 14 design variables, namely, C_1, C_2, C_3, C_4, L_1, L_2, ..., L_{10}. The nominal solution was achieved by minimax optimization after 35 iterations (about 3 minutes on a Sun

SPARCstation 1). The gain and VSWR before and after optimization are shown in Fig. 18. The values of the design variables before and after optimization are listed in Table V.

The minimax nominal design is then used as the starting point for yield optimization. We use the PBMs for both the MESFETs and the passive elements. Since all devices are made from the same material and on the same wafer, they share common parameters. All three MESFETs have the same values for the critical electric field, saturation velocity, relative dielectric constant, built-in potential, low-field mobility and high-field diffusion coefficient. All the MIM capacitors have the same dielectric film, and all bulk resistors have the same sheet resistance. The geometrical parameters can have different values for different devices, including the gate length, gate width, and channel thickness of the MESFETs, the metal plate area of the MIM capacitors, and the number of turns of the spiral inductors. The doping densities of the MESFETs are also considered as independent parameters.

A total of 37 parameters are considered as statistical variables. They include the gate length, gate width, channel thickness and doping density of the MESFETs, as well as the geometrical parameters of the passive elements. The mean values and standard deviations of the statistical variables are listed in Table VI. Correlations are also included in the statistical model. The most significant correlations are the ones between the same parameters from the same devices. For instance, the gate lengths of the three MESFETs are strongly correlated. The correlation matrix is given in Table VII.

The number of turns of the 10 spiral inductors, the metal plate area of the 4 MIM capacitors, and the channel thickness and doping density of the MESFETs are chosen as the variables for yield optimization. At the starting point (i.e., the minimax nominal design), the yield was 47.5% as estimated by Monte Carlo analysis with 200 statistical outcomes. The yield was improved to 78.5% at the solution of the yield optimization (about 3 hours CPU time on a Sun SPARCstation 1). The solution is given in Table VIII. The Monte Carlo sweep of gain and VSWR before and after yield optimization are shown in Figs. 19 and 20, respectively.

VII. THE OSA90/hope SYSTEM [127]

OSA90/hope is a new CAD system offering simulation, modeling, statistical analysis, nominal and yield optimization capabilities for general linear and nonlinear circuits. We have used the OSA90/hope system as the principal vehicle for implementing our theory and developing our examples. We present an example of two-dimensional nonlinear MESFET field simulation after a brief outline of the features of OSA90/hope pertinent to our presentation.

A. OSA90/hope: A Brief Outline

Both ECMs [2–4, 166] and PBMs for FET devices [144] are available in OSA90/hope. Hence we are able to compare different models in an otherwise identical environment. Most significantly, using the user-defined model features in OSA90/hope, we can easily create and verify new models, such as the Ladbrooke FET model [159] presented in this paper.

In OSA90/hope, DC, small-signal AC and large-signal harmonic balance analyses are analytically unified. This allows us to obtain consistent DC, small- and large-signal responses from the same model, as well as to optimize circuits to meet multidimensional specifications, such as simultaneous small- and large-signal specifications [165].

OSA90/hope employs *FAST* sensitivity analysis which combines the simplicity of *PAST* and the efficiency of *EAST* (see Section IV) to provide gradients for ℓ_1, ℓ_2 and minimax optimization of linear and nonlinear circuits. Yield optimization is carried out by a sophisticated one-sided ℓ_1 algorithm [72].

One of the unique features of OSA90/hope is the Datapipe technology for functionally connecting external simulators. It utilizes UNIX interprocess pipes for high-speed data communication between OSA90/hope and external programs. This effectively offers an open software architecture for the user to incorporate external modules into the optimization shell. Since such modules are separate programs, they can be independently developed and modified. The basic structure of the Datapipe feature is illustrated in Fig. 21.

Datapipe is especially suitable for integrating separate programs each of which is responsible

for a portion of the overall task. The external programs can concentrate on intensive number crunching operations such as solving physics-based model equations and field theoretic models, while OSA90/hope interacts with the user and provides pre-, inter- and post-processing capabilities for the inputs to and outputs from the external programs.

We demonstrate the potential of this system by a field-based MESFET simulation example.

B. Field-Based MESFET Simulation and Modeling

A two-dimensional (2D) field-based MESFET simulation has been carried out. We connect OSA90/hope with an external 2D field simulator using Datapipe. The parameters of the MESFET device are specified in the OSA90/hope input file and are passed to the field simulator. Simulation is carried out by the field simulator externally and the results are returned to OSA90/hope for further use. We first perform 2D field simulation of a MESFET and then we use the Plessey model [167] to match the simulation results and create the corresponding equivalent circuit model.

The MESFET model used for 2D field simulation is based on numerical techniques presented by Reiser [130] and Snowden *et al.* [133]. It is a 2D drift-diffusion MESFET model which is relatively mature and easy to implement. The schematic diagram of the MESFET is shown in Fig. 1.

The model formulation is based on [130,133]: (1) neglecting minority carriers, (2) neglecting thermal generation and recombination effects, and (3) describing the carrier flow by the diffusion equations. The basic model equations are described by equations (1)-(5) in Section II. The diffusion coefficient D is determined from the Einstein relation

$$D = \frac{kT}{q}\mu \tag{85}$$

with Boltzman constant k and the absolute temperature T. The electron mobility μ is considered to be a function of the electric field magnitude E as described by an empirical expression [133]

$$\mu(E) = \frac{300\mu_0}{T}\left[\frac{1 + \dfrac{8.5\times10^4 E^3}{\mu_0 E_0^4(1 - 5.3\times10^4 T)}}{1 + \left(\dfrac{E}{E_0}\right)^4}\right] \tag{86}$$

where

$$\mu_0 = \frac{0.8}{1 + \sqrt{\dfrac{N}{10^{23}}}} \tag{87}$$

2D Poisson's equations and current continuity equations with the boundary conditions approximated according to the physical nature of the device borders are solved using the finite difference method to simulate the internal device physics.

A 0.5×300μm GaAs MESFET is considered. Its physical parameters, as listed in Table IX, and the approximated doping profile, as listed in Table X, are passed from OSA90/hope to the 2D field simulator for time-domain simulation. The required DC steady-state simulation results are then returned from the 2D field simulator to OSA90/hope. 56 DC bias points are simulated. It took about 14 hours of CPU time on a Sun SPARCstation 1 to finish the simulation. The simulated DC results are shown in Fig. 22 by circles.

We apply a FET model (modified Statz model) from Plessey [167] to match the results of the 2D field MESFET simulation. The model is a pre-programmed user model in OSA90/hope. The model equation can be written as

$$I_{ds} = \frac{I_{dss}(V_{gs} - V_t)^2}{1 + b(V_{gs} - V_t)}(1 + \lambda V_{ds})\tanh(\alpha V_{ds}) + \left(1 + \frac{V_{ds}}{V_{t1}}\right) G_{dst} V_{ds}\tanh(\alpha V_{ds}) \tag{88}$$

where

$$V_{t1} = V_t(1 - \beta V_{ds}) \tag{89}$$

I_{dss}, V_t, G_{dst}, b, α, β and λ are the parameters to be determined.

The efficient ℓ_1 optimization is invoked to extract the model parameters. All 56 simulated

points are to be matched. It took about 3 minutes of CPU time for the parameter extraction optimization on a Sun SPARCstation 1. The model parameter values before and after optimization are listed in Table XI. The DC characteristics simulated by the 2D field simulator and those calculated by the Plessey model are compared in Fig. 22.

VIII. CONCLUSIONS

We have presented our approach towards physics-oriented microwave circuit optimization. We have addressed device modeling, parameter extraction, nonlinear simulation, nominal design, statistical modeling and yield optimization.

Analytical large-signal physical models of MESFETs have been discussed and new developments presented. Nonlinear circuit analysis with physics-based models integrated into the HB equations have been described. New approximations to the behaviour of electron drift velocity versus electric field have been made. Results have been implemented in a model originated by Khatibzadeh and Trew. *FAST* has been shown to be suitable for high speed gradient calculations for circuit optimization employing physical, geometrical and process-related parameters of devices as design variables. Simultaneous, hierarchical, nonlinear, yield-driven optimization has been demonstrated.

Statistical modeling of active devices with physics-based models has been explored. Our procedure has been illustrated through new implementations of the Ladbrooke model and the Khatibzadeh and Trew model. The results from the Ladbrooke model have demonstrated the feasibility of using PBMs for statistical modeling, though further investigation of the Khatibzadeh and Trew model for statistical purposes is needed. Physics-based statistical models have been applied to physics-based yield-driven optimization suitable for MMICs. Both passive and active elements have been related through common process-oriented statistical parameters.

Effective multidimensional quadratic functions have been employed to simultaneously approximate responses and gradients. Our novel theoretical developments have been incorporated into OSA90/hope and HarPE. They are thereby available to the microwave community. OSA90/hope's

novel Datapipe structure constitutes the first microwave CAD product of its kind. The open architecture feature enables device and circuit designers to solve a variety of relevant linear/nonlinear/statistical modeling, simulation and optimization problems with both circuit and physical parameters.

APPENDIX

STATISTICAL DEFINITIONS AND FORMULAS [168]

Suppose we have a set of random parameters ϕ_i, $i = 1, 2, ..., n$. The statistical characteristics of these parameters can be described by their mean values, variances, correlations, and even higher moments. The mean value for each parameter ϕ_i is defined as

$$E(\phi_i) = \nu_{\phi_i} = \int_{-\infty}^{\infty} \phi_i p(\phi_i) d\phi_i \tag{A1}$$

where $p(\phi_i)$ is the probability density function. The variance of ϕ_i is defined as

$$D(\phi_i) = E\{(\phi_i - \nu_{\phi_i})^2\} = \sigma_{\phi_i}^2 = \int_{-\infty}^{\infty} (\phi_i - \nu_{\phi_i})^2 p(\phi_i) d\phi_i \tag{A2}$$

The positive square root of the variance is called the standard deviation and is denoted by σ. The covariance of parameters ϕ_i and ϕ_j is defined as

$$cov(\phi_i, \phi_j) = E\{(\phi_i - \nu_{\phi_i})(\phi_j - \nu_{\phi_j})\} \tag{A3}$$

and the correlation coefficient between ϕ_i and ϕ_j is then defined as

$$r_{\phi_i \phi_j} = \frac{cov(\phi_i, \phi_j)}{\sigma_{\phi_i} \sigma_{\phi_j}} \tag{A4}$$

ACKNOWLEDGEMENTS

The authors would like to express their appreciation to Dr. Rolf H. Jansen of Jansen Microwave, Ratingen, Germany, Guest Co-Editor of this Special Issue, for several significantly inspiring discussions. The authors thank Dr. Robert J. Trew of North Carolina State University, Raleigh, NC, for useful discussions and providing essential data. The authors acknowledge some original work done by Dr. Jian Song which has been integrated into our presentation. Thanks are also due to Dr. D. Mike Brookbanks of Plessey Research Caswell, Northamptonshire, England, for technical discussions and generously providing measurement data. Thanks are also extended to his colleague Dr. Ron G. Arnold. Thanks are due to Dr. Peter H. Ladbrooke of GaAs Code Ltd., Cambridge, England, for helpful discussions and comments [169]. Finally, thanks are extended to Dr. Walter R. Curtice of W.R. Curtice Consulting, Princeton Junction, NJ, for helpful criticisms and discussions.

REFERENCES

[1] W.R. Curtice, "A MESFET model for use in the design of GaAs integrated circuits," *IEEE Trans. Microwave Theory Tech.*, vol. MTT-28, 1980, pp. 448-456.

[2] W.R. Curtice and M. Ettenberg, "A nonlinear GaAs FET model for use in the design of output circuits for power amplifiers," *IEEE Trans. Microwave Theory Tech.*, vol. MTT-33, 1985, pp. 1383-1394.

[3] A. Materka and T. Kacprzak, "Computer calculation of large-signal GaAs FET amplifier characteristics," *IEEE Trans. Microwave Theory Tech.*, vol. MTT-33, 1985, pp. 129-135.

[4] H. Statz, P. Newman, I.W. Smith, R.A. Pucel and H.A. Haus, "GaAs FET device and circuit simulation in SPICE," *IEEE Trans. Electron Devices*, vol. ED-34, 1987, pp. 160-169.

[5] V.D. Hwang and T. Itoh, "An efficient approach for large-signal modeling and analysis of GaAs MESFET," *IEEE Trans. Microwave Theory Tech.*, vol. MTT-35, 1987, pp. 396-402.

[6] J.W. Bandler, S.H. Chen, S. Ye and Q.J. Zhang, "Integrated model parameter extraction using large-scale optimization concepts," *IEEE Trans. Microwave Theory Tech.*, vol. 36, 1988, pp. 1629-1638.

[7] J.W. Bandler, Q.J. Zhang, S. Ye and S.H. Chen, "Efficient large-signal FET parameter extraction using harmonics," *IEEE Trans. Microwave Theory Tech.*, vol. 37, 1989, pp. 2099-2108.

[8] J.W. Bandler, Q.J. Zhang and Q. Cai, "Nonlinear circuit optimization with dynamically integrated physical device models," *IEEE Int. Microwave Symp. Dig.* (Dallas, TX), 1990, pp. 303-306.

[9] R.J. Gilmore and M.B. Steer, "Nonlinear circuit analysis using the method of harmonic balance-a review of the art. Part I. introductory concepts," *Int. J. Microwave and Millimetre-Wave Computer-Aided Engineering*, vol. 1, 1991, pp. 22-37.

[10] L.O. Chua and P. Lin, *Computer-Aided Analysis of Electronic Circuits: Algorithms and Computational Techniques.* Engelwood Cliffs, NJ: Prentice-Hall, 1975.

[11] S. Skelboe, "Computation of the periodic steady-state response of nonlinear networks by extrapolation methods," *IEEE Trans. Circuits Syst.*, vol. CAS-27, 1980, pp. 161-175.

[12] S. Skelboe, "Time-domain steady-state analysis of nonlinear electrical systems," *Proc. IEEE*, vol. 70, 1982, pp. 1210-1228.

[13] J. Vlach and K. Singhal, *Computer Methods for Circuit Analysis and Design.* New York: Van Nostrand Reinhold, 1983.

[14] A.K. Jastrzebski and M.I. Sobhy, "Analysis of microwave circuits using state-space approach," *Proc. IEEE Int. Symp. Circuits Syst.* (Montreal, Canada), 1984, pp. 1119-1122.

[15] M.I. Sobhy and A.K. Jastrzebski, "Direct integration methods of nonlinear microwave circuits," *Proc. 15th European Microwave Conf.* (Paris, France), 1985, pp. 1110-1118.

[16] L.W. Nagel and D.O. Pederson, *SPICE (Simulation Program with Integrated Circuit Emphasis)*, Electronics Research Laboratory, University of California, Memo ERL-M382, April, 1973.

[17] S.W. Director, "A method for quick determination of the periodic steady-state in nonlinear networks," *Proc. 9th Allerton Conf. Circuits Syst. Theory*, (Urbana, IL), 1971, pp. 131-139.

[18] T.J. Aprille, Jr. and T.N. Trick, "Steady-state analysis of nonlinear circuits with periodic inputs," *Proc. IEEE*, vol. 60, 1972, pp. 108-114.

[19] T.J. Aprille, Jr. and T.N. Trick, "A computer algorithm to determine the steady-state response of nonlinear oscillators," *IEEE Trans. Circuit Theory*, vol. CT-19, 1972, pp. 354-360.

[20] F.R. Colon and T.N. Trick, "Fast periodic steady-state analysis for large-signal electronic circuits," *IEEE J. Solid-State Circuits*, vol. SC-8, 1973, pp. 260-269.

[21] S.W. Director and K.W. Current, "Optimization of forced nonlinear periodic circuits," *IEEE Trans. Circuits Syst.*, vol. CAS-23, 1976, pp. 329-335.

[22] M.S. Nakhla and F.H. Branin, Jr., "Determining the periodic response of nonlinear systems by a gradient method," *Int. J. Circuit Theory Appl.*, vol. 5, 1977, pp. 255-273.

[23] M.B. Steer, C.R. Chang and G.W. Rhyne, "Computer-aided analysis of nonlinear microwave circuits using frequency-domain nonlinear analysis techniques: the state of the art," *Int. J. Microwave and Millimetre-Wave Computer-Aided Engineering*, vol. 1, 1991, pp. 181-200.

[24] R.G. Sea, "An algebraic formula for amplitudes of intermodulation products involving an arbitrary number of frequencies," *Proc. IEEE*, vol. 56, 1968, pp. 1388-1389.

[25] R.G. Sea and A.G. Vacroux, "On the computation of intermodulation products for a power series nonlinearity," *Proc. IEEE*, 1969, pp. 337-338.

[26] M.B. Steer and P.J. Khan, "An algebraic formula for the output of a system with large-signal multifrequency excitation," *Proc. IEEE*, 1983, pp. 177-179.

[27] G.W. Rhyne, M.B. Steer and B.D. Bates, "Frequency-domain nonlinear circuit analysis using generalized power series," *IEEE Trans. Microwave Theory Tech.*, vol. MTT-36, 1988, pp. 379-387.

[28] V. Volterra, *Theory of Functionals and of Integral and Integro-Differential Equations*. London: Blackie & Son, 1930.

[29] E. Bedrosian and S.O. Rice, "The output properties of Volterra systems (nonlinear systems with memory) driven by harmonic and Gaussian inputs," *Proc. IEEE*, vol. 59, 1971, pp. 1688-1707.

[30] J.J. Bussgang, L. Ehrman and J.W. Graham, "Analysis of nonlinear systems with multiple inputs," *Proc. IEEE*, vol. 62, 1974, pp. 1088-1119.

[31] D.D. Weiner and J.F. Spina, *Sinusoidal Analysis and Modeling of Weakly Nonlinear Circuits*. New YorK: Van Nostrand Reinhold, 1980.

[32] I.W. Sandberg, "Expansions for nonlinear systems," *Bell Syst. Tech. J.*, vol. 61, 1982, pp. 159–199.

[33] S.A. Maas, "A general-purpose computer program for the Volterra-series analysis of nonlinear microwave circuits," *IEEE Int. Microwave Symp. Dig.* (New York, NY), 1988, pp. 311–314.

[34] A. Ushida and L.O. Chua, "Frequency-domain analysis of nonlinear circuits driven by multi-tone signals," *IEEE Trans. Circuits Syst.*, vol. CAS-31, 1984, pp. 766–779.

[35] J.H. Haywood and Y.L. Chow, "Intermodulation distortion analysis using a frequency-domain harmonic balance technique," *IEEE Trans. Microwave Theory Tech.*, vol. MTT-36, 1988, pp. 1251–1257.

[36] C.R. Chang, M.B. Steer and G.W. Rhyne, "Frequency-domain spectral balance using the arithmetic operator method," *IEEE Trans. Microwave Theory Tech.*, vol. MTT-37, 1989, pp. 1681–1688.

[37] G.L. Heiter, "Characterization of nonlinearities in microwave devices and systems," *IEEE Trans. Microwave Theory Tech.*, vol. MTT-21, 1973, pp. 797–805.

[38] R.B. Swerdlow, "Analysis of intermodulation noise in frequency converters by Volterra series," *IEEE Trans. Microwave Theory Tech.*, vol. MTT-26, 1978, pp. 305–313.

[39] R.S. Tucker, "Third-order intermodulation distortion and gain compression in GaAs FET's," *IEEE Trans. Microwave Theory Tech.*, vol. MTT-27, 1979, pp. 400–408.

[40] R.A. Minasian, "Intermodulation distortion analysis of MESFET amplifiers using Volterra series representation," *IEEE Trans. Microwave Theory Tech.*, vol. MTT-28, 1980, pp. 1–8.

[41] C.L. Law and C.S. Aitchison, "Prediction of wide-band power performance of MESFET distributed amplifiers using the Volterra series representation," *IEEE Trans. Microwave Theory Tech.*, vol. MTT-34, 1986, pp. 1308–1317.

[42] G.W. Rhyne and M.B. Steer, "Generalized power series analysis of intermodulation distortion in a MESFET amplifier: simulation and experiment," *IEEE Trans. Microwave Theory Tech.*, vol. MTT-35, 1987, pp. 1248–1255.

[43] Y. Hu, J. Obregon and J.C. Mollier, "Nonlinear analysis of microwave FET oscillators using Volterra series," *IEEE Trans. Microwave Theory Tech.*, vol. 37, 1989, pp. 1689–1693.

[44] C.R. Chang and M.B. Steer, "Frequency-domain nonlinear microwave circuit simulation using the arithmetic operator method," *IEEE Trans. Microwave Theory Tech.*, vol. 38, 1990, pp. 1139–1143.

[45] W.J. Cunningham, *Introduction to Nonlinear Analysis.* New York: McGraw-Hill, 1958.

[46] J.C. Lindenlaub, "An approach for finding the sinusoidal steady-state response of nonlinear systems," *Proc. 7th Allerton Conf. Circuit Syst. Theory* (Chicago, IL), 1969, pp. 323–327.

[47] M.S. Nakhla and J. Vlach, "A piecewise harmonic-balance technique for determination of periodic response of nonlinear systems," *IEEE Trans. Circuits Syst.*, vol. CAS-23, 1976, pp. 85–91.

[48] A.I. Mees, *Dynamics of Feedback Systems*. New York: Wiley, 1981.

[49] V. Rizzoli, A. Lipparini, and E. Marazzi, "A general-purpose program for nonlinear microwave circuit design," *IEEE Trans. Microwave Theory Tech.*, vol. 31, 1983, pp. 762–770.

[50] K. S. Kundert and A. Sangiovanni-Vincentelli, "Simulation of nonlinear circuits in the frequency domain," *IEEE Trans. Computer-Aided Design*, vol. CAD-5, 1986, pp. 521–535.

[51] V. Rizzoli, C. Cecchetti, A. Lipparini, and F. Mastri, "General-purpose harmonic balance analysis of nonlinear microwave circuits under multitone excitation," *IEEE Trans. Microwave Theory Tech.*, vol. 36, 1988, pp. 1650–1660.

[52] R.J. Gilmore and M.B. Steer, "Nonlinear circuit analysis using the method of harmonic balance–a review of the art. Part II. advanced concepts," *Int. J. Microwave and Millimetre-Wave Computer-Aided Engineering*, vol. 1, 1991, pp. 159–180.

[53] F. Filicori, V.A. Monaco and C. Naldi, "Simulation and design of microwave class-C amplifiers through harmonic analysis," *IEEE Trans. Microwave Theory Tech.*, vol. MTT-27, 1979, pp. 1043–1051.

[54] R.G. Hicks and P.J. Khan, "Numerical analysis of subharmonic mixers using accurate and approximate models," *IEEE Trans. Microwave Theory Tech.*, vol. MTT-30, 1982, pp. 2113–2120.

[55] W.R. Curtice, "Nonlinear analysis of GaAs MESFET amplifiers, mixers, and distributed amplifiers using harmonic balance technique," *IEEE Trans. Microwave Theory Tech.*, vol. 35, 1987, pp. 441–447.

[56] B.R. Epstein, S.M. Perlow, D.L. Rhodes, J.L. Schepps, M.M. Ettenberg and R. Barton, "Large-signal MESFET characterization using harmonic balance," *IEEE Int. Microwave Symp. Dig.* (New York, NY), 1988, pp. 1045–1048.

[57] S. El-Rabaie, J.A.C. Stewart, V.F. Fusco and J.J. McKeown, "A novel approach for the large signal analysis and optimisation of microwave frequency doublers", *IEEE Int. Microwave Symp. Dig.* (New York, NY), 1988, pp. 1119–1122.

[58] P.W. Van Der Walt, "Efficient technique for solving nonlinear mixer pumping problem," *Electronics Lett.*, vol 21, 1985, pp. 899–900.

[59] V.D. Hwang, Y-C. Shih, H.M. Le and T. Itoh, "Nonlinear modeling and verification of MMIC amplifiers using the waveform-balance method", *IEEE Trans. Microwave Theory Tech.*, vol. 37, 1989, pp. 2125–2133.

[60] R. Gilmore, "Nonlinear circuit design using the modified harmonic balance algorithm", *IEEE Trans. Microwave Theory Tech.*, vol. MTT-34, 1986, pp. 1294–1307.

[61] A. Lipparini, E. Marazzi and V. Rizzoli, "A new approach to the computer-aided design of nonlinear networks and its application to microwave parametric frequency dividers," *IEEE Trans. Microwave Theory Tech.*, vol. MTT-30, 1982, pp. 1050–1058.

[62] V. Rizzoli and A. Neri, "State of the art and present trends in nonlinear microwave CAD techniques", *IEEE Trans. Microwave Theory Tech.*, vol. 36, 1988, pp. 343–365.

[63] J.W. Bandler, Q.J. Zhang, J. Song and R.M. Biernacki, "FAST gradient based yield optimization of nonlinear circuits", *IEEE Trans. Microwave Theory Tech.*, vol. 38, 1990, pp. 1701–1710.

[64] R.H. Jansen, R.G. Arnold and I.G. Eddison, "A comprehensive CAD approach to the design of MMICs up to mm–wave frequencies", *IEEE Trans. Microwave Theory Tech.*, vol. 36, 1988, pp. 208–219.

[65] R.H. Jansen, I.G. Eddison and R.G. Arnold, "Recent developments in CAD of high packing density MMICs", *MIOP 1989* (Sindelfingen, West Germany), 1989, Paper 1.3.

[66] R.H. Jansen, "Progress in passive and active MMIC device modeling", *Workshop on Progress in Microwave CAD and in CAD Applications Dig.* (Ratingen, West Germany), 1989, pp. 173–196.

[67] F.A. Myers, "Advanced GaAs MMIC elements and circuits", *Workshop on Progress in Microwave CAD and in CAD Applications Dig.* (Ratingen, West Germany), 1989, pp. 197–203.

[68] R. Goyal, M. Golio and W. Thomann, "Device Modeling", in *Monolithic Microwave Integrated Circuits: Technology & Design*, R. Goyal Ed. Boston: Artech House, 1989, Chapter 4.

[69] E.D. Cohen, "MIMIC from the Department of Defense perspective", *IEEE Trans. Microwave Theory Tech.*, vol. 38, 1990, pp. 1171–1174.

[70] C.M. Snowden, "Microwave and millimeter–wave device and circuit design based on physical modeling," *Int. J. on Microwave and Millimetre-Wave Computer-Aided Engineering*, vol. 1, 1991, pp. 4–21.

[71] R.J. Trew, "MESFET models for microwave CAD applications," *Int. J. on Microwave and Millimetre-Wave Computer-Aided Engineering*, vol. 1, 1991, pp. 143–158.

[72] J.W. Bandler and S.H. Chen, "Circuit optimization: the state of the art", *IEEE Trans. Microwave Theory Tech.*, vol. 36, 1988, pp. 424–443.

[73] J. Purviance, D. Criss and D. Monteith, "FET model statistics and their effects on design centering and yield prediction for microwave amplifiers," *IEEE Int. Microwave Symp. Dig.* (New York, NY), 1988, pp. 315–318.

[74] R.W. Dutton, D.A. Divekar, A.G. Gonzalez, S.E. Hansen and D.A. Antoniadis, "Correlation of fabrication process and electrical device parameter variations," *IEEE J. Solid-State Circuits*, vol. SC–12, 1977, pp. 349–355.

[75] D.A. Divekar, R.W. Dutton and W.J. McCalla, "Experimental study of Gummel–Poon model parameter correlations for bipolar junction transistors," *IEEE J. Solid-State Circuits*, vol. SC–12, 1977, pp. 552–559.

[76] M.A. Styblinski, "Factor analysis model of resistor correlations for monolithic integrated circuits," *Proc. IEEE Int. Symp. Circuits Syst.* (Tokyo, Japan), 1977, pp. 776–777.

[77] P.J. Rankin, "Statistical modeling for integrated circuits," *IEE Proc.*, vol. 129, Pt. G, No. 4, 1982, pp. 186–191.

[78] S. Freeman, "Statistical techniques for calibrating simulation models of analog circuits and devices," *Proc. IEEE Int. Symp. Circuits Syst.* (Montreal, Canada), 1984, pp. 684–688.

[79] S. Liu and K. Singhal, "A statistical model for MOSFETs," *Proc. IEEE Int. Conf. Computer-Aided Design* (Santa Clara, CA), 1985, pp. 78–80.

[80] P. Cox, P. Yang, S.S. Mahant-Shetti and P. Chatterjee, "Statistical modeling for efficient parametric yield estimation of MOS VLSI circuits," *IEEE Trans. Electron Devices*, vol. ED–32, 1985, pp. 471–478.

[81] N. Herr and J.J. Barnes, "Statistical circuit simulation modeling of CMOS VLSI," *IEEE Trans. Computer-Aided Design*, vol. CAD–5, 1986, pp. 15–22.

[82] C.J.B. Spanos and S.W. Director, "Parameter extraction for statistical IC process characterization," *IEEE Trans. Computer-Aided Design*, vol. CAD–5, 1986, pp. 66–78.

[83] J.E. Purviance, M.C. Petzold and C. Potratz, "A linear statistical FET model using principal component analysis," *IEEE Trans. Microwave Theory Tech.*, vol. 37, 1989, pp. 1389–1394.

[84] J.W. Bandler, R.M. Biernacki, S.H. Chen, J. Loman, M. Renault and Q.J. Zhang, "Combined discrete/normal statistical modeling of microwave devices," *Proc. European Microwave Conf.* (Wembley, England), 1989, pp. 205–210.

[85] J. Purviance, M. Meehan and D. Collins, "Properties of FET parameter statistical data bases," *IEEE Int. Microwave Symp. Dig.* (Dallas, TX), 1990, pp. 567–570.

[86] J.W. Bandler, R.M. Biernacki, S.H. Chen, J. Song, S. Ye and Q.J. Zhang, "Statistical modeling of GaAs MESFETs," *IEEE Int. Microwave Symp. Dig.* (Boston, MA), 1991, pp. 87–90.

[87] A.R. Jha, R. Goyal and B. Manz, "Introduction," in *Monolithic Microwave Integrated Circuits: Technology & Design*, R. Goyal Ed. Boston: Artech House, 1989, Chapter 1.

[88] B.J. Karafin, "The optimum assignment of component tolerances for electrical networks," *Bell Syst. Tech. J.*, vol. 50, 1971, pp. 1225–1242.

[89] J.F. Pinel and K.A. Roberts, "Tolerance assignment in linear networks using nonlinear programming," *IEEE Trans. Circuit Theory*, vol. CT–19, 1972, pp. 475–479.

[90] J.W. Bandler, "Optimization of design tolerances using nonlinear programming," *Proc. 6th Princeton Conf. on Information Science and Systems* (Princeton, NJ), 1972, pp. 655–659. Also in *Computer-Aided Filter Design*, G. Szentirmai, Ed. New York: IEEE Press, 1973.

[91] J.W. Bandler, "The tolerance problem in optimal design," *Proc. European Microwave Conf.* (Brussels, Belgium), 1973, Paper A.13.1.(I).

[92] J.W. Bandler, "Optimization of design tolerances using nonlinear programming," *J. Optimization Theory and Applications*, vol. 14, 1974, pp. 99–114.

[93] J.W. Bandler, P.C. Liu and H. Tromp, "A nonlinear programming approach to optimal design centering, tolerancing and tuning," *IEEE Trans. Circuits Syst.*, vol. CAS–23, 1976, pp. 155–165.

[94] J.W. Bandler, P.C. Liu and H. Tromp, "Integrated approach to microwave design," *IEEE Trans. Microwave Theory Tech.*, vol. MTT-24, 1976, pp. 584–591.

[95] S.W. Director and G.D. Hachtel, "The simplicial approximation approach to design centering," *IEEE Trans. Circuits Syst.*, vol. CAS-24, 1977, pp. 363–372.

[96] J.W. Bandler and H.L. Abdel-Malek, "Optimal centering, tolerancing, and yield determination via updated approximations and cuts," *IEEE Trans. Circuits Syst.*, vol. CAS-25, 1978, pp. 853–871.

[97] E. Polak and A. Sangiovanni-Vincentelli, "Theoretical and computational aspects of the optimal design centering, tolerancing, and tuning problem," *IEEE Trans. Circuits Syst.*, vol. CAS-26, 1979, pp. 795–813.

[98] H.L. Abdel-Malek and J.W. Bandler, "Yield optimization for arbitrary statistical distributions: Part I-theory," *IEEE Trans. Circuits Syst.*, vol. CAS-27, 1980, pp. 245–253.

[99] R.S. Soin and R. Spence, "Statistical exploration approach to design centering," *Proc. IEE*, vol. 127, pt. G., 1980, pp. 260–269.

[100] M.A. Styblinski and A. Ruszczynski, "Stochastic approximation approach to statistical circuit design," *Electronics Lett.*, vol. 19, 1980, pp. 300–302.

[101] K. Singhal and J.F. Pinel, "Statistical design centering and tolerancing using parametric sampling," *IEEE Trans. Circuits Syst.*, vol. CAS-28, 1981, pp. 692–702.

[102] T. Downs, A.S. Cook and G. Rogers, "A partitioning approach to yield estimation for large circuit and systems," *IEEE Trans. Circuits Syst.*, vol. CAS-31, 1984, pp. 472–485.

[103] J.W. Bandler and A.E. Salama, "Functional approach to microwave postproduction tuning," *IEEE Trans. Microwave Theory Tech.*, vol. MTT-33, 1985, pp. 302–310.

[104] A.J. Strojwas and A. Sangiovanni-Vincentelli, Eds., *IEEE Trans. Computer-Aided Design*, Special Issue on Statistical Design of VLSI Circuits, vol. CAD-5, 1986, pp. 5–169.

[105] P. Yang, D.E. Hocevar, P.F. Cox, C. Machala and P.K. Chatterjee, "An integrated and efficient approach for MOS VLSI statistical circuit design," *IEEE Trans. Computer-Aided Design*, vol. CAD-5, 1986, pp. 5–14.

[106] M.L. Stein, "An efficient method of sampling for statistical circuit design," *IEEE Trans. Computer-Aided Design*, vol. CAD-5, 1986, pp. 23–29.

[107] M.A. Styblinski, "Problems of yield gradient estimation for truncated probability density functions," *IEEE Trans. Computer-Aided Design*, vol. CAD-5, 1986, pp. 30–38.

[108] M.A. Styblinski and L.J. Opalski, "Algorithms and software tools for IC yield optimization based on fundamental fabrication parameters," *IEEE Trans. Computer-Aided Design*, vol. CAD-5, 1986, pp. 79–89.

[109] J.P. Spoto, W.T. Coston and C.P. Hernandez, "Statistical integrated circuit design and characterization," *IEEE Trans. Computer-Aided Design*, vol. CAD-5, 1986, pp. 90–103.

[110] S.R. Nassif, A.J. Strojwas and S.W. Director, "A methodology for worst-case analysis of integrated circuits," *IEEE Trans. Computer-Aided Design*, vol. CAD-5, 1986, pp. 104-113.

[111] W. Maly, A.J. Strojwas and S.W. Director, "VLSI yield prediction and estimation: a unified framework," *IEEE Trans. Computer-Aided Design*, vol. CAD-5, 1986, pp. 114-130.

[112] D. Riley and A. Sangiovanni-Vincentelli, "Models for a new profit-based methodology for statistical design of integrated circuits," *IEEE Trans. Computer-Aided Design*, vol. CAD-5, 1986, pp. 131-169.

[113] L.J. Opalski and M.A. Styblinski, "Generalization of yield optimization problem: maximum income approach," *IEEE Trans. Computer-Aided Design*, vol. CAD-5, 1986, pp. 346-360.

[114] Y. Aoki, H. Masuda, S. Shimada and S. Sato, "A new design-centering methodology for VLSI device development," *IEEE Trans. Computer-Aided Design*, vol. CAD-6, 1987, pp. 452-461.

[115] T.K. Yu, S.M. Kang, I.N. Hajj and T.N. Trick, "Statistical performance modeling and parametric yield estimation of MOS VLSI," *IEEE Trans. Computer-Aided Design*, vol. CAD-6, 1987, pp. 1013-1022.

[116] D.E. Hocevar, P.F. Cox and P. Yang, "Parametric yield optimization for MOS circuit blocks," *IEEE Trans. Computer-Aided Design*, vol. CAD-7, 1988, pp. 645-658.

[117] J.W. Bandler, R.M. Biernacki, S.H. Chen, M. Renault, J. Song and Q.J. Zhang, "Yield optimization of large scale microwave circuits," *Proc. European Microwave Conf.* (Stockholm, Sweden), 1988, pp. 255-260.

[118] R.M. Biernacki, J.W. Bandler, J. Song and Q.J. Zhang, "Efficient quadratic approximation for statistical design," *IEEE Trans. Circuits Syst.*, vol. 36, 1989, pp. 1449-1454.

[119] J.W. Bandler, Q.J. Zhang, J. Song and R.M. Biernacki, "Yield optimization of nonlinear circuits with statistically characterized devices," *IEEE Int. Microwave Symp. Dig.* (Long Beach, CA), 1989, pp. 649-652.

[120] M.D. Meehan, T. Wandinger and D.A. Fisher, "Accurate design centering and yield prediction using the 'truth model'," *IEEE Int. Microwave Symp. Dig.* (Boston, MA), 1991, pp. 1201-1204.

[121] J. Purviance and M. Meehan, "CAD for statistical analysis and design of microwave circuits", *Int. J. Microwave and Millimeter-Wave Computer-Aided Engineering*, vol. 1, 1991, pp. 59-76.

[122] R.J. Gilmore, M. Eron and T. Zhang, "Yield optimization of a MMIC distributed amplifier using physically-based device models," *IEEE Int. Microwave Symp. Dig.* (Boston, MA), 1991, pp. 1205-1208.

[123] J.W. Bandler, Q. Cai, R.M. Biernacki, S.H. Chen and Q.J. Zhang, "Physics-based design and yield optimization of MMICs," *Proc. European Microwave Conf.* (Stuttgart, Germany), 1991.

[124] C.H. Corbex, A.F. Gerodolle, S.P. Martin and A.R. Poncet, "Data structuring for process and device simulations," *IEEE Trans. Computer-Aided Design*, vol. 7, 1988, pp. 489-500.

[125] J.R.F. McMacken and S.G. Chamberlain, "CHORD: a modular semiconductor device simulation development tool incorporating external network models," *IEEE Trans. Computer-*

Aided Design, vol. 8, 1989, pp. 826–836.

[126] P. Lloyd, H.K. Dirks, E.J. Prendergast and K. Singhal, "Technology CAD for competitive products," *IEEE Trans. Computer-Aided Design*, vol. 9, 1990, pp. 1209–1216.

[127] *OSA90/hope*, Optimization Systems Associates Inc., P.O. Box 8083, Dundas, Ontario, Canada L9H 5E7, 1991.

[128] *HarPE*, Optimization Systems Associates Inc., P.O. Box 8083, Dundas, Ontario, Canada L9H 5E7, 1991.

[129] D.P. Kennedy and R.R. O'Brien, "Computer aided two dimensional analysis of the junction field-effect transistor," *IBM J. Res. Devel.*, vol. 14, 1970, pp. 95–116.

[130] M. Reiser, "A two-dimensional numerical FET model for DC, ac and large-signal analysis," *IEEE Trans. Electron Devices*, vol. ED-20, 1973, pp. 35–45.

[131] T. Wada and J. Frey, "Physical basis of short-channel MESFET operation," *IEEE Trans. Electron Devices*, vol. ED-26, 1979, pp. 476–490.

[132] W.R. Curtice and Y.H. Yun, "A temperature model for the GaAs MESFET," *IEEE Trans. Electron Devices*, vol. ED-28, 1981, pp. 954–962.

[133] C.M. Snowden, M.J. Hawes and D.V. Morgan, "Large-signal modeling of GaAs MESFET operation," *IEEE Trans. Electron Devices*, vol. ED-30, 1983, pp. 1817–1824.

[134] C.M. Snowden and D. Loret, "Two-dimensional hot-electron models for shot-gate-length GaAs MESFETs," *IEEE Trans. Electron Devices*, vol. ED-34, 1987, pp. 212–223.

[135] W. Shockley, "A unipolar 'field-effect' transistor", *Proc. IRE*, vol. 40, 1952, pp. 1365–1376.

[136] J.A. Turner and B.L.H. Wilson, "Implications of carrier velocity saturation in a gallium arsenide field-effect transistor," *Proc. Symp. Gallium Arsenide*, 1968, pp. 195–204.

[137] A.B. Grebene and S.K. Ghandhi, "General theory for pinched operation of the junction-gate FET," *Solid-State Electronics*, vol. 12, 1969, pp. 573–589.

[138] K. Lehovec and R. Zuleeg, "Voltage-current characteristics of GaAs J-FETs in the hot electron range", *Solid-State Electronics*, vol. 13, 1970, pp. 1415–1426.

[139] A. Pucel, A. Haus and H. Statz, "Signal and noise properties of gallium arsenide microwave field-effect transistors", in *Advances in Electronics and Electron Physics*, vol. 38. New York: Academic Press, 1975, pp. 195–265.

[140] T.H. Chen and M.S. Shur, "Analytic models for ion-implanted GaAs FET's," *IEEE Trans. Electron Devices*, vol. ED-32, 1985, pp. 18–28.

[141] T.H. Chen and M.S. Shur, "A capacitance model for GaAs MESFETs," *IEEE Trans. Electron Devices*, vol. ED-32, 1985, pp. 883–891.

[142] K. Yamaguchi and H. Kodera, "Drain conductance of junction gate FET's in the hot electron range", *IEEE Trans. Electron Devices*, vol. ED-23, 1976, pp. 545–553.

[143] A. Madjar and F.J. Rosenbaum, "A large-signal model for the GaAs MESFET", *IEEE Trans. Microwave Theory Tech.*, vol. MTT-29, 1981, pp. 781-788.

[144] M.A. Khatibzadeh and R.J. Trew, "A large-signal, analytic model for the GaAs MESFET", *IEEE Trans. Microwave Theory Tech.*, vol. 36, 1988, pp. 231-238.

[145] C.S. Chang and D.Y.S. Day, "Analytic theory for current-voltage characteristics and field distribution of GaAs MESFET's", *IEEE Trans. Electron Devices*, vol. 36, 1989, pp. 269-280.

[146] J.G. Ruch and G.S. Kino, "Measurement of the velocity-field characteristic of gallium arsenide", *Appl. Phys. Lett.*, vol. 10, 1967, pp. 40-42.

[147] P.A. Houston and A.G.R. Evans, "Electron drift velocity in n-GaAs at high electric fields", *Solid-State Electronics*, vol. 20, 1977, pp. 197-204.

[148] M.A. Khatibzadeh, "Large-signal modeling of gallium-arsenide field-effect transistors", Ph.D. dissertation, North Carolina State University, Raleigh, NC, 1987.

[149] H. Fukui, "Determination of the basic device parameters of a GaAs MESFET," *Bell Syst. Tech. J.*, vol. 58, 1979, pp. 771-797.

[150] W.R. Curtice, "GaAs MESFET modeling and nonlinear CAD," *IEEE Trans. Microwave Theory Tech.*, vol. 36, 1988, pp. 220-230.

[151] Measurement data provided by Plessey Research Caswell Ltd., Caswell, Towcester, Northamptonshire, England NN12 8EQ, 1990.

[152] J.W. Bandler, W. Kellermann and K. Madsen, "A nonlinear l_1 optimization algorithm for design, modeling, and diagnosis of networks", *IEEE Trans. Circuits Syst.*, vol. CAS-34, 1987, pp. 174-181.

[153] J.W. Bandler, S.H. Chen, S. Daijavad and K. Madsen, "Efficient optimization with integrated gradient approximations," *IEEE Trans. Microwave Theory Tech.*, vol. 36, 1988, pp. 444-455.

[154] C.G. Broyden, "A class of methods for solving nonlinear simultaneous equations," *Mathematics of Computation*, vol. 19, 1965, pp. 577-593.

[155] M.J.D. Powell, "A Fortran subroutine for unconstrained minimization, requiring first derivatives of the objective functions," Atomic Energy Research Establishment, Harwell, Berkshire, England, Rep. AERE-R. 6469, 1970, pp. 20-27.

[156] J.W. Bandler, Q.J. Zhang and R.M. Biernacki, "A unified theory for frequency domain simulation and sensitivity analysis of linear and nonlinear circuits," *IEEE Trans. Microwave Theory Tech.*, vol. 36, 1988, pp. 1661-1669.

[157] J.W. Bandler, Q.J. Zhang and R.M. Biernacki, "Practical, high-speed gradient computation for harmonic balance simulators," *IEEE Int. Microwave Symp. Dig.* (Long Beach, CA), 1989, pp. 363-366.

[158] H.L. Abdel-Malek and J.W. Bandler, "Yield optimization for arbitrary statistical distributions: Part II-implementation," *IEEE Trans. Circuits and Syst.*, vol. CAS-27, 1980, pp. 253-262.

[159] P.H. Ladbrooke, *MMIC Design: GaAs FETs and HEMTs*. Norwood, MA: Artech House, 1989.

[160] I.J. Bahl, "Transmission Lines and Lumped Elements", in *Microwave Solid State Circuit Design*, I.J. Bahl and P. Bhartia, Eds. New York: Wiley, 1988, Chapter 2.

[161] R.M. Biernacki and M.A. Styblinski, "Statistical circuit design with a dynamic constraint approximation scheme," *Proc. IEEE Int. Symp. Circuits Syst.* (San Jose, CA), 1986, pp. 976–979.

[162] J.W. Bandler, R.M. Biernacki, S.H. Chen, J. Song, S. Ye and Q.J. Zhang, "Gradient quadratic approximation scheme for yield-driven design," *IEEE Int. Microwave Symp. Dig.* (Boston, MA), 1991, pp. 1197–1200.

[163] C. Kermarrec and C. Rumelhard, "Microwave monolithic integrated circuits", in *GaAs MESFET Circuit Design*, R. Soares Ed. Boston: Artech House, 1988, Chapter 9.

[164] J.W. Bandler, W. Kellermann and K. Madsen, "A superlinearly convergent minimax algorithm for microwave circuit design", *IEEE Trans. Microwave Theory Tech.*, vol. MTT-33, 1985, pp. 1519–1530.

[165] J.W. Bandler, R.M. Biernacki, S.H. Chen, J. Song, S. Ye and Q.J. Zhang, "Analytically unified DC/small-signal/large-signal circuit design," *IEEE Trans. Microwave Theory Tech.*, vol. 39, 1991, pp. 1076–1082.

[166] I.E. Getreu, *CAD of Electronic Circuits 1: Modeling the Bipolar Transistor*. Amsterdam: Elsevier Scientific Publishing Company, 1978.

[167] D.M. Brookbanks, Plessey Research Caswell Ltd., Caswell, Towcester, Northamptonshire, England NN12 8EQ, Private Communication, 1990.

[168] H.C. de Graaff and F.M. Klaassen, *Compact Transistor Modelling for Circuit Design*. New York: Springer-Verlag Wien, 1990.

[169] P.H. Ladbrooke, GaAs Code Ltd., St John's Innovation Center, Cowley, Cambridge CB4 4WS, U.K., Private Communication, July 15, 1991.

TABLE I

INTRINSIC PARAMETERS OF THE MODEL

Parameter	Notation	Unit
Gate Length	L	μm
Gate Width	W	μm
Channel Thickness	a	μm
Doping Density	N_d	cm^{-3}
Critical Electric Field	E_c	kV/cm
Saturation Velocity	v_s	cm/s
Relative Dielectric Constant	ε_r	———
Built-in Potential	V_{bi}	V
Low-Field Mobility	μ_0	$cm^2/(Vs)$
High-Field Diffusion Coefficient	D_0	cm^2/s

TABLE II

PARAMETER EXTRACTION FOR THE KHATIBZADEH AND TREW MODEL

Parameter	Before Optimization	After Optimization	Plessey Data [151]
L(μm)	0.551	0.5002	0.551
W(μm)	300.0	305.19	300.0
$N_d(cm^{-3})$	2.235×10^{17}	2.3706×10^{17}	2.235×10^{17}
a(μm)	0.200	0.1282	---
$R_g(\Omega)$	2.500	4.0826	---
$R_d(\Omega)$	3.000	10.000	---
$R_s(\Omega)$	2.500	2.6645	---
L_g(nH)	0.010	0.0337	---
L_d(nH)	0.010	0.0001	---
L_s(nH)	0.010	0.0428	---
C_x(pF)	2.000	3.0000	---
C_{ge}(pF)	0.100	0.1473	---
C_{de}(pF)	0.100	0.0540	---
$G_{ds}(1/\Omega)$	0.003	0.0038	---

Other intrinsic parameters are fixed as

$E_c = 3.36kV/cm$ $\quad v_s = 1.344\times10^7 cm/s$

$V_{bi} = 0.7V$ $\quad \mu_0 = 4000cm^2/(Vs)$

$D_0 = 10cm^2/s$ $\quad \varepsilon_r = 12.9$

TABLE III

STATISTICAL PARAMETERS FOR THE LADBROOKE AND THE KHATIBZADEH AND TREW MODELS

Ladbrooke Model			Khatibzadeh and Trew Model		
Para.	Mean	Dev.(%)	Para.	Mean	Dev.(%)
$L(\mu m)$	0.5559	2.93	$L(\mu m)$	0.5496	1.29
$a(\mu m)$	0.1059	3.64	$a(\mu m)$	0.1310	1.38
$N_d(cm^{-3})$	3.140E17	1.71	$N_d(cm^{-3})$	2.219E17	0.98
$v_s(cm/s)$	7.608E6	3.48	$W(\mu cm)$	295.24	1.48
$V_{B0}(V)$	0.6785	4.94	$V_{bi}(V)$	0.699	1.62
a_0	1.031	7.03	$\mu_0(cm^2/Vs)$	3932	1.16
$r_{01}(1/A^2)$	1.090E-2	0.44	$E_c(kV/cm)$	3.255	1.38
$r_{02}(V)$	628.2	6.86	$R_D(\Omega)$	4.001	0.06
$r_{03}(\Omega)$	13.99	0.44	$R_S(\Omega)$	1.697	0.17
$R_G(\Omega)$	3.392	4.99	$R_G(\Omega)$	3.500	0.12
$L_{G0}(nH)$	2.414E-2	20.7	$L_G(nH)$	2.94E-2	0.13
$L_D(nH)$	6.117E-2	18.6	$L_D(nH)$	8.0E-3	0.06
$L_S(nH)$	2.209E-2	10.6	$L_S(nH)$	3.9E-2	0.85
$G_{DS}(1/\Omega)$	2.163E-3	2.72	$G_{DS}(1/\Omega)$	3.6E-3	0.61
$C_{DS}(pF)$	5.429E-2	2.71	$C_{DE}(pF)$	5.27E-2	0.78
			$C_{GE}(pF)$	0.1504	1.89

TABLE IV

MEAN VALUES AND STANDARD DEVIATIONS OF MEASURED AND SIMULATED S-PARAMETERS AT 11GHZ

	Measured S-parameters [151]		Simulated S-parameters			
			Ladbrooke Model		Khatibzadeh and Trew Model	
	Mean	Dev.(%)	Mean	Dev.(%)	Mean	Dev.(%)
$\|S_{11}\|$	0.773	.988	.7856	.764	.8085	0.32
$\angle S_{11}$	-114.3	1.36	-119.3	1.10	-116.2	0.69
$\|S_{21}\|$	1.919	.802	1.679	1.34	1.834	1.22
$\angle S_{21}$	93.35	.856	94.06	.835	91.69	0.33
$\|S_{12}\|$	.0765	3.77	.07542	3.68	.0785	2.07
$\angle S_{12}$	34.00	2.51	31.98	2.33	31.61	0.94
$\|S_{22}\|$	0.5957	1.48	.5838	1.54	.5446	1.11
$\angle S_{22}$	-38.69	2.10	-36.86	1.42	-40.64	0.98

TABLE V

DESIGN VARIABLES FOR NOMINAL DESIGN

Design Variable	Before Optimization	After Optimization	Design Variable	Before Optimization	After Optimization
C_1(pF)	0.62	0.335	L_4(nH)	0.31	0.432
C_2(pF)	0.55	1.446	L_5(nH)	0.59	0.460
C_3(pF)	0.45	0.367	L_6(nH)	0.31	0.263
C_4(pF)	0.62	0.308	L_7(nH)	0.13	0.154
L_1(nH)	1.59	1.001	L_8(nH)	1.00	0.664
L_2(nH)	2.36	2.073	L_9(nH)	0.59	0.552
L_3(nH)	0.31	0.460	L_{10}(nH)	2.36	1.652

TABLE VI

ASSUMED DISTRIBUTIONS FOR STATISTICAL VARIABLES

Variable	Mean	Dev.(%)	Variable	Mean	Dev.(%)
$N_d(cm^{-3})$	2.0×10^{17}	7.0	$d(\mu m)$	0.1	4.0
$L_G(\mu m)$	1.0	3.5	$S_{C1}(\mu m^2)$	532.7	3.5
$A_G(\mu m)$	0.24	3.5	$S_{C2}(\mu m^2)$	2278.9	3.5
$W_G(\mu m)$	400	2.0	$S_{C3}(\mu m^2)$	583.1	3.5
$W_L(\mu m)$	20	3.0	$S_{C4}(\mu m^2)$	468.7	3.5
$S_L(\mu m)$	10	3.0			

The doping density N_d, gate length L_G, channel thickness A_G and gate width W_G of the three MESFETs have the same distribution. The conductor width W_L and spacing S_L of the 10 spiral inductors L_1, L_2, ..., L_{10} have the same distribution. d is the thickness of the dielectric film for all MIM capacitors. S_{Ci} is the area of the metal plate of MIM capacitor C_i.

TABLE VII

ASSUMED PARAMETER CORRELATIONS FOR THE THREE MESFETS

	GA_1	GL_1	GW_1	N_{d1}	GA_2	GL_2	GW_2	N_{d2}	GA_3	GL_3	GW_3	N_{d3}
GA_1	1.00	0.00	0.00	-0.25	0.80	0.00	0.00	-0.20	0.78	0.00	0.00	-0.10
GL_1	0.00	1.00	0.00	-0.10	0.00	0.80	0.00	-0.05	0.00	0.78	0.00	-0.05
GW_1	0.00	0.00	1.00	0.00	0.00	0.00	0.80	0.00	0.00	0.00	0.78	0.00
N_{d1}	-0.25	-0.10	0.00	1.00	-0.20	-0.05	0.00	0.80	-0.15	-0.05	0.00	0.78
GA_2	0.80	0.00	0.00	-0.20	1.00	0.00	0.00	-0.25	0.80	0.00	0.00	-0.20
GL_2	0.00	0.80	0.00	-0.05	0.00	1.00	0.00	-0.10	0.00	0.80	0.00	-0.10
GW_2	0.00	0.00	0.80	0.00	0.00	0.00	1.00	0.00	0.00	0.00	0.80	0.00
N_{d2}	-0.20	-0.05	0.00	0.80	-0.25	-0.10	0.00	1.00	-0.20	-0.05	0.00	0.80
GA_3	0.78	0.00	0.00	-0.15	0.80	0.00	0.00	-0.20	1.00	0.00	0.00	-0.25
GL_3	0.00	0.78	0.00	-0.05	0.00	0.80	0.00	-0.05	0.00	1.00	0.00	-0.10
GW_3	0.00	0.00	0.78	0.00	0.00	0.00	0.80	0.00	0.00	0.00	1.00	0.00
N_{d3}	-0.10	-0.05	0.00	0.78	-0.20	-0.10	0.00	0.80	-0.25	-0.10	0.00	1.00

TABLE VIII

DESIGN VARIABLES FOR YIELD OPTIMIZATION

Design Variable	Before Optimization	After Optimization	Design Variable	Before Optimization	After Optimization
$A_G(\mu m)$	0.24	0.243	n_{L3}	2.33	2.04
$N_d(cm^{-3})$	2.0×10^{17}	2.03×10^{17}	n_{L4}	2.29	2.34
$S_{C1}(\mu m^2)$	532.7	552.2	n_{L5}	2.32	2.39
$S_{C2}(\mu m^2)$	2278.9	1910.2	n_{L6}	1.84	2.08
$S_{C3}(\mu m^2)$	583.1	554.2	n_{L7}	1.49	1.50
$S_{C4}(\mu m^2)$	468.7	477.2	n_{L8}	2.65	2.82
n_{L1}	2.88	2.79	n_{L9}	2.43	2.48
n_{L2}	3.98	4.11	n_{L10}	3.27	3.35

n_{Li} is the number of turns of the spiral inductor L_i.

TABLE IX

PARAMETERS FOR THE 0.5μm GATE LENGTH GaAs MESFET

Source Length	0.15μm
Source-Gate Gap	0.50μm
Gate Length	0.50μm
Drain-Gate Gap	0.60μm
Drain Length	0.15μm
Gate Width	300μm
Channel Thickness	0.15μm
Buffer Layer Thickness	0.20μm
Substrate Thickness	0.05μm
Schottky Barrier Height	0.80V
Temperature	350K
Doping of Active Layer	$1.5\times10^{23}m^{-3}$
Doping at Contacts	$3.7\times10^{23}m^{-3}$
Substrate Impurity Level	$1.0\times10^{10}m^{-3}$

TABLE X

DOPING PROFILE FOR THE 0.5μm GaAs MESFET

Grid No.	Doping (m^{-3})	Grid No.	Doping (m^{-3})
0	1.5000×10^{23}	17	1.7705×10^{22}
1	1.5000×10^{23}	18	7.7109×10^{21}
2	1.5000×10^{23}	19	3.1290×10^{21}
3	1.5000×10^{23}	20	1.2247×10^{21}
4	1.5000×10^{23}	21	4.7939×10^{20}
5	1.5000×10^{23}	22	1.9453×10^{20}
6	1.5000×10^{23}	23	8.4721×10^{19}
7	1.5000×10^{23}	24	4.0886×10^{19}
8	1.5000×10^{23}	25	2.2485×10^{19}
9	1.5000×10^{23}	26	1.4419×10^{19}
10	1.5000×10^{23}	27	1.0967×10^{19}
11	1.5000×10^{23}	28	1.0000×10^{19}
12	1.5000×10^{23}	29	1.0000×10^{19}
13	1.3676×10^{23}	30	1.0000×10^{19}
14	1.0402×10^{23}	31	1.0000×10^{19}
15	6.6710×10^{22}	32	1.0000×10^{19}
16	3.6687×10^{22}		

TABLE XI

PARAMETER VALUES FOR THE PLESSEY MODEL

Parameter	Before Optimization	After Optimization
I_{dss}(mA)	60	52.49
V_t(V)	-4.0	-4.10
b(V)	1.5E-3	2.23E-6
$\lambda(1/\Omega)$	0.01	0.011
$\alpha(1/V)$	14.5	3.316
$G_{dst}(1/\Omega)$	3.0E-3	2.47E-3
$\beta(1/V)$	16.5	20.0

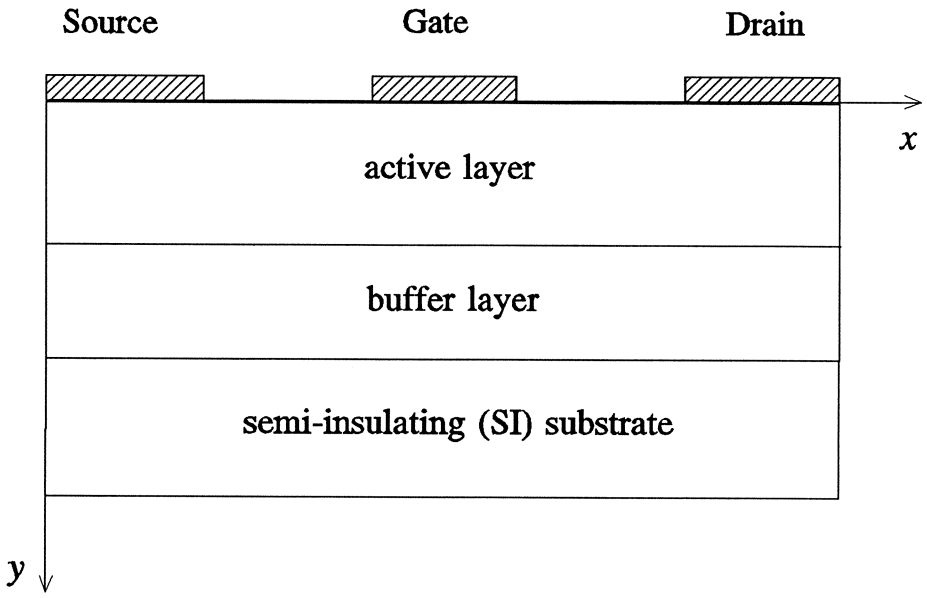

Fig. 1. A simplified cross-section of a MESFET.

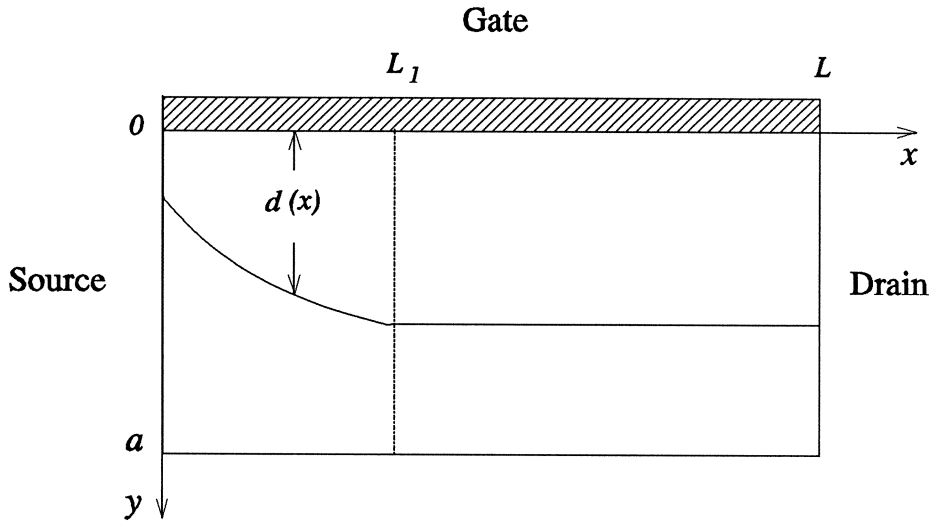

Fig. 2. Active region of the MESFET.

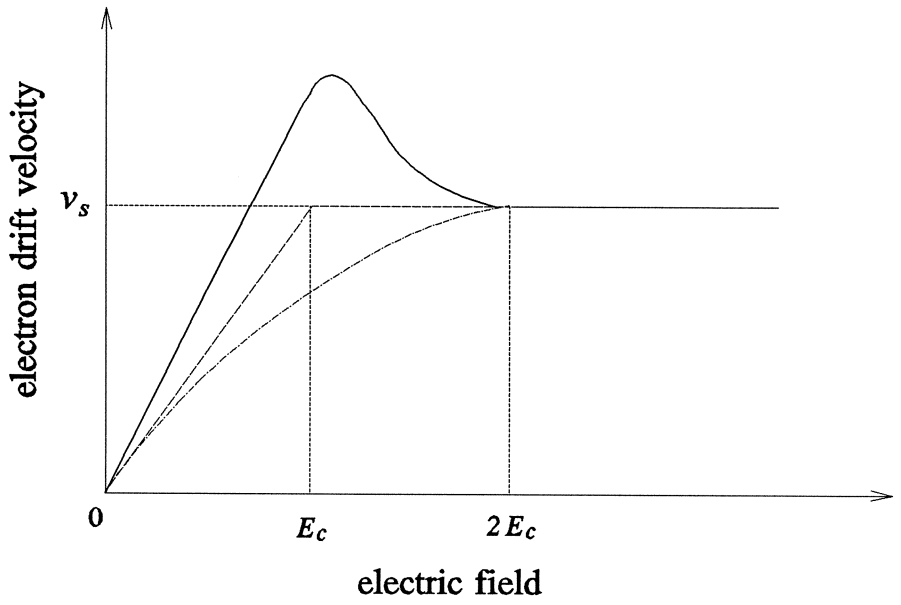

Fig. 3. Electron drift velocity versus electric field: (——) actual v-E curve, (---) piecewise linear approximation and (-•-) quadratic approximation.

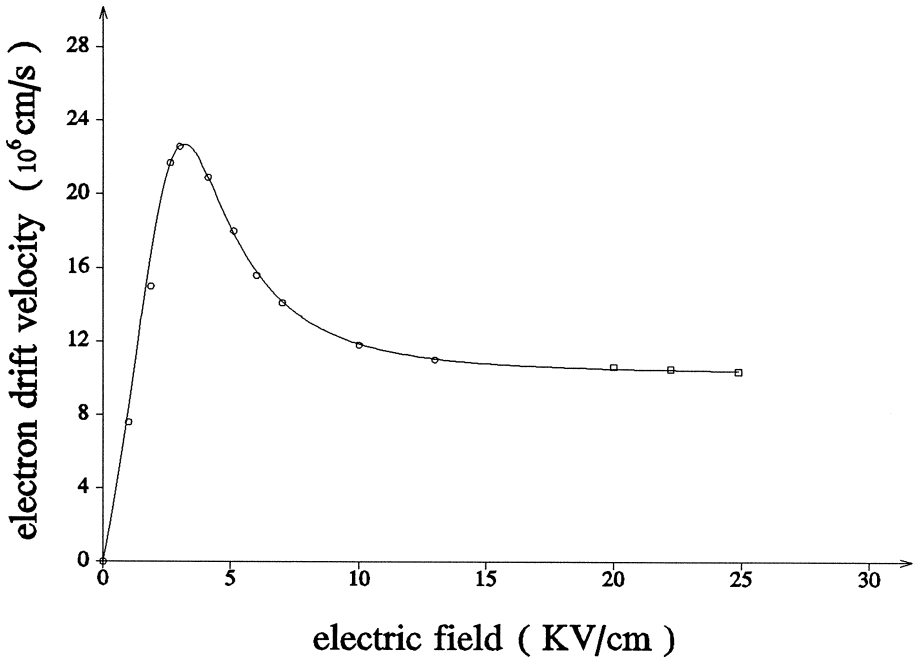

Fig. 4. Comparison of calculated and experimental v-E data for GaAs: (——) calculated from Equation (12), (○) experimental datafrom Ruch and Kino [146], and (□) experimental data from Houseton and Evans [147].

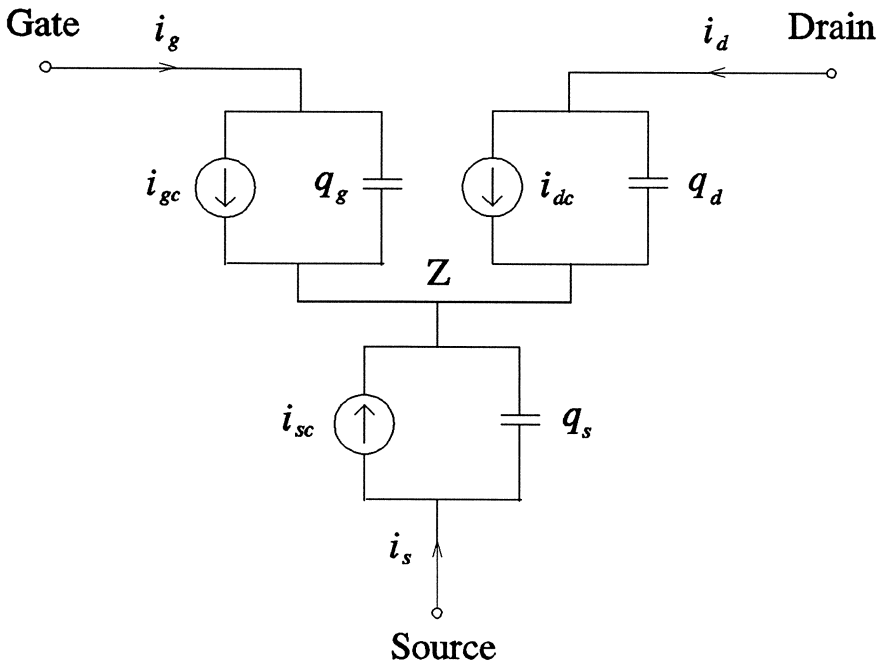

Fig. 5. Equivalent circuit for the intrinsic model.

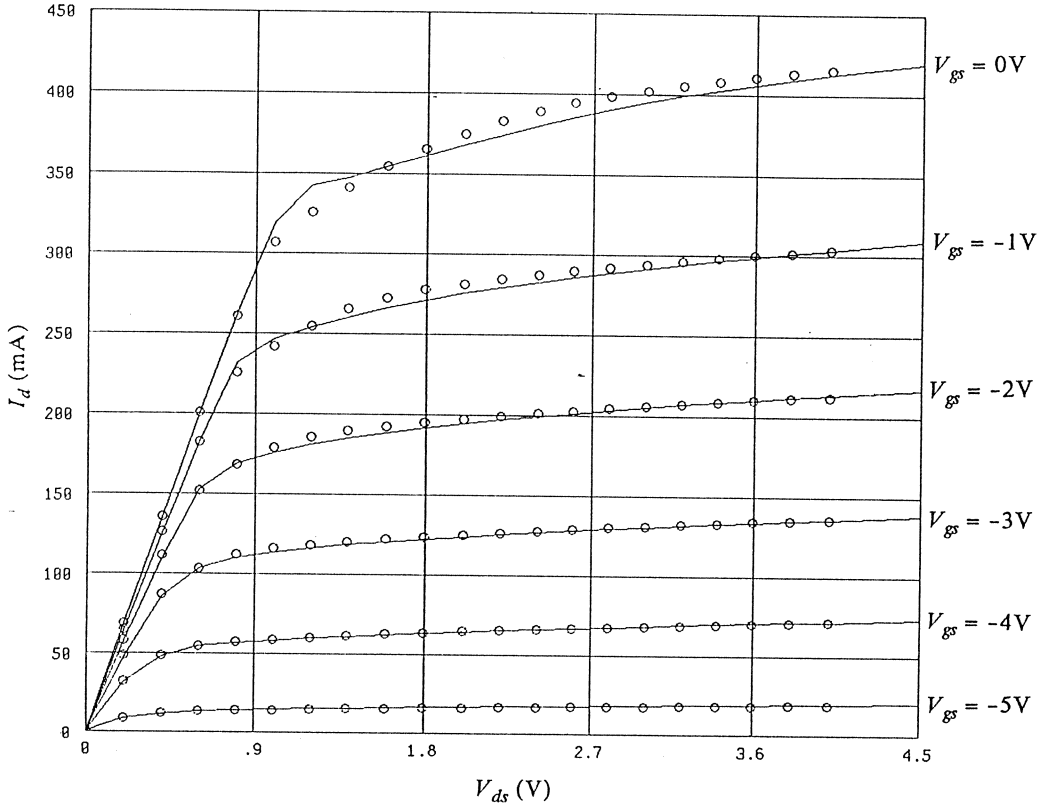

Fig. 6. Comparison of our approach with that of Khatibzadeh's on DC characteristics: (——) our results and (O) Khatibzadeh's results [148].

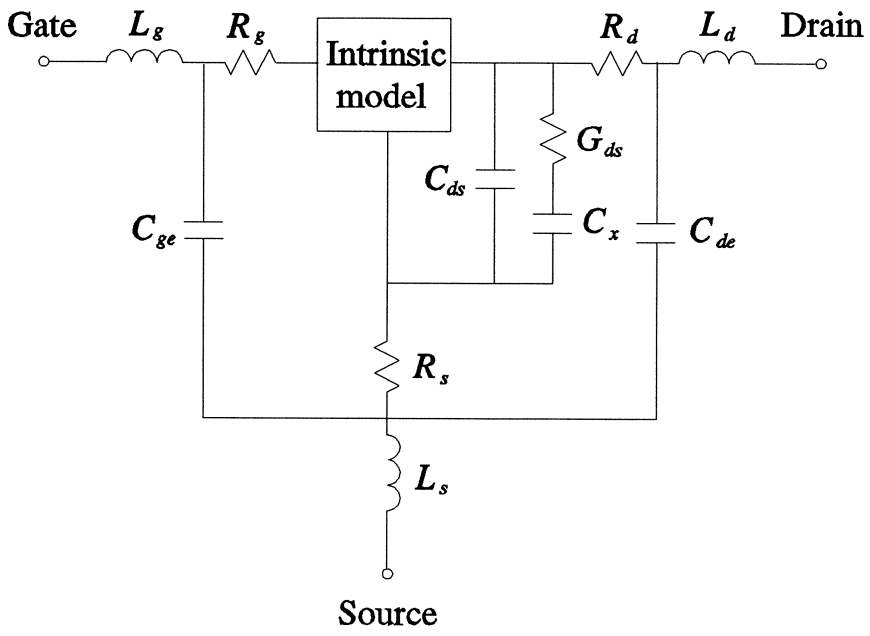

Fig. 7. Circuit topology for parameter extraction showing the intrinsic FET and its associated extrinsic elements.

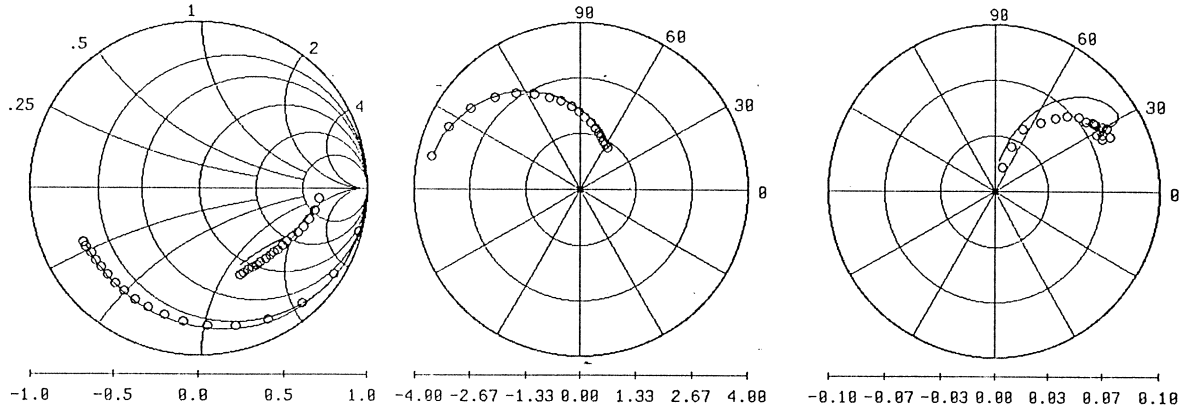

(a)

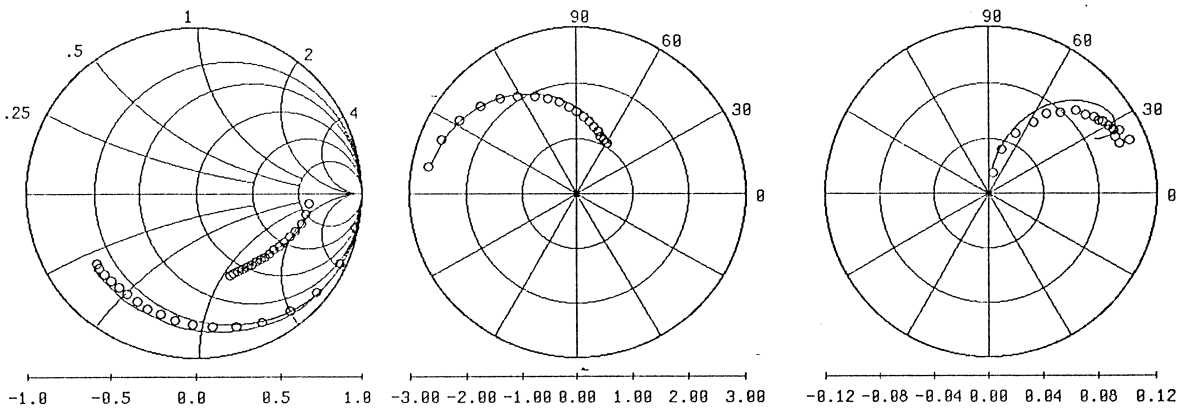

(b)

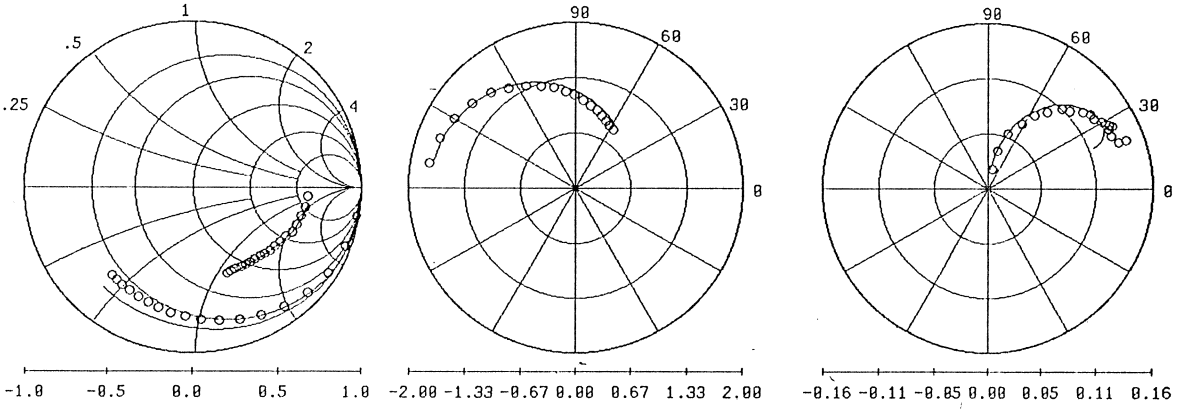

(c)

Fig. 8. Comparison of measured (O) and calculated (——) S-parameters at 3 bias points for parameter extraction. (a) gate bias 0V, (b) gate bias -0.84V and (c) gate bias -1.54V. Drain bias is 5V.

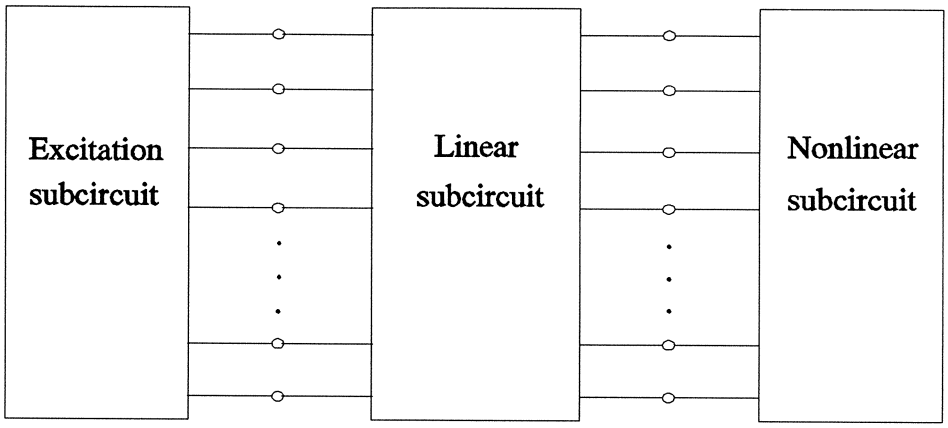

Fig. 9. Partition of the circuit for harmonic balance simulation.

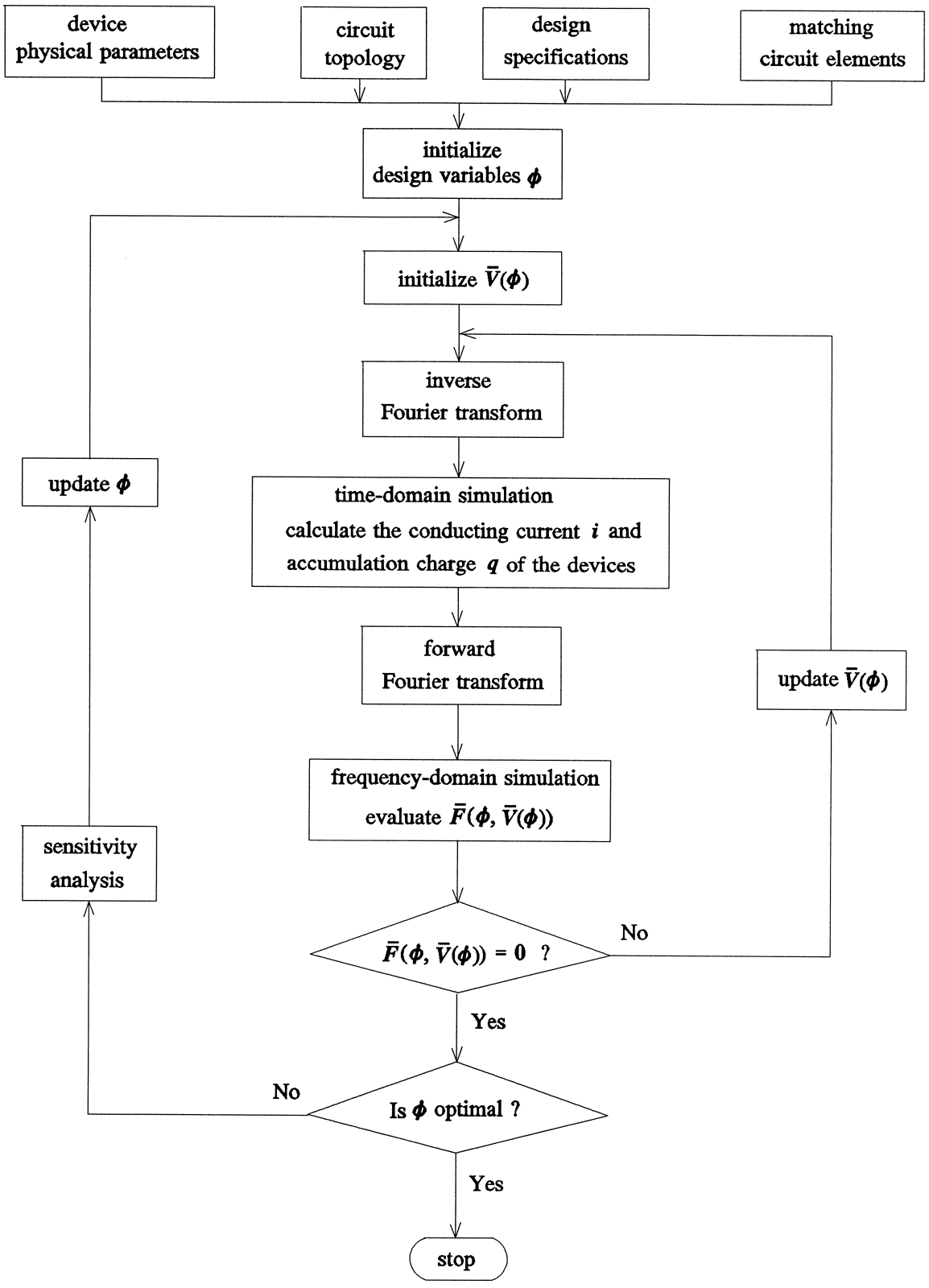

Fig. 10. Flowchart for design optimization of nonlinear FET circuits using HB.

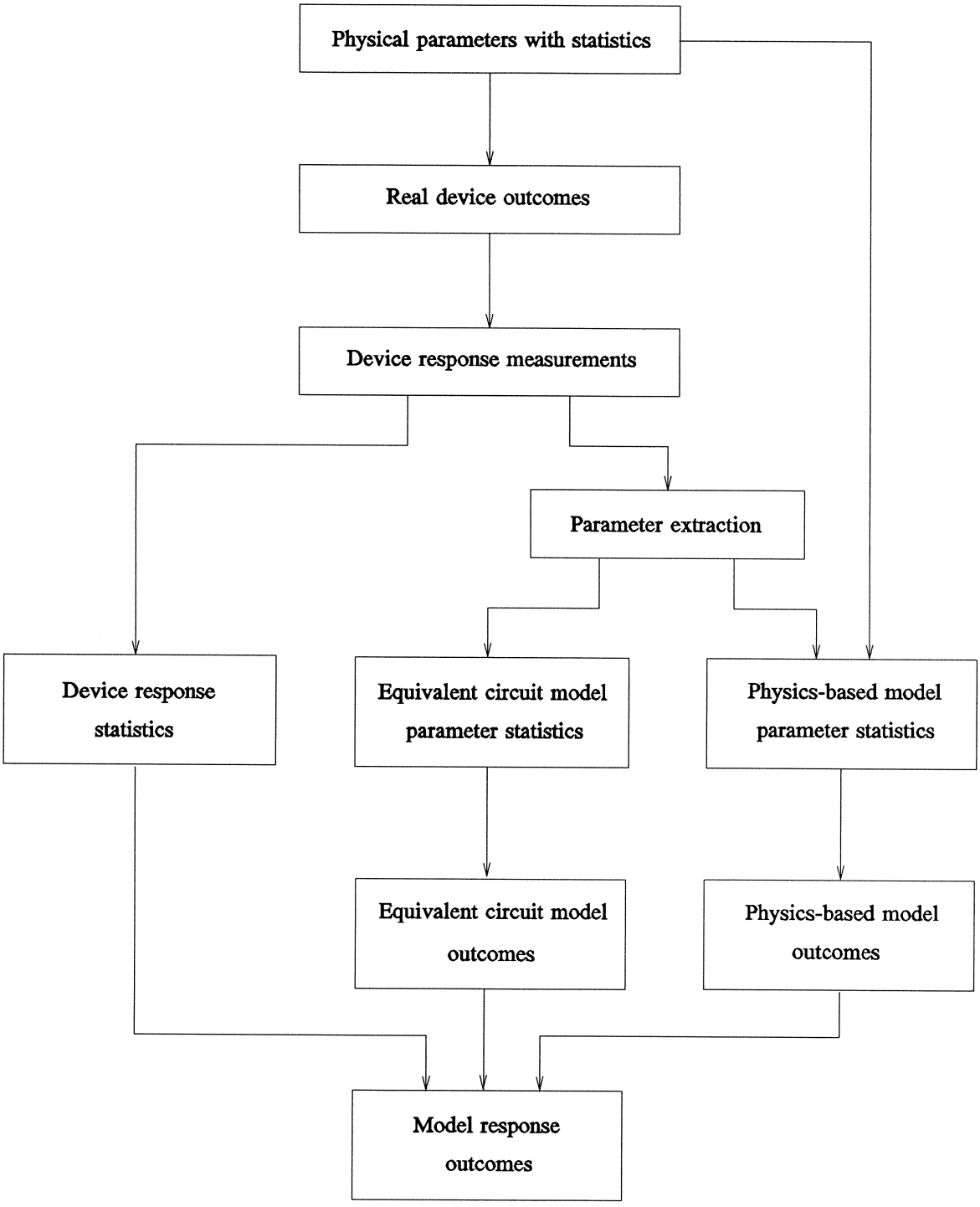

Fig. 11. Hierarchical statistics.

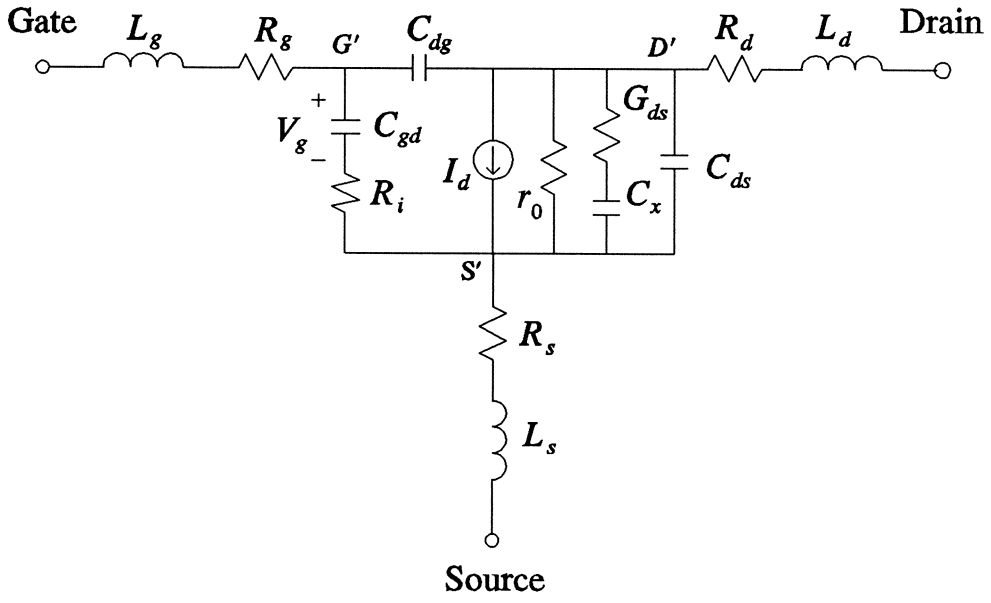

Fig. 12. Topology for the Ladbrooke GaAs MESFET small-signal model where $I_d = g_m V_g \exp(-j\omega\tau)$.

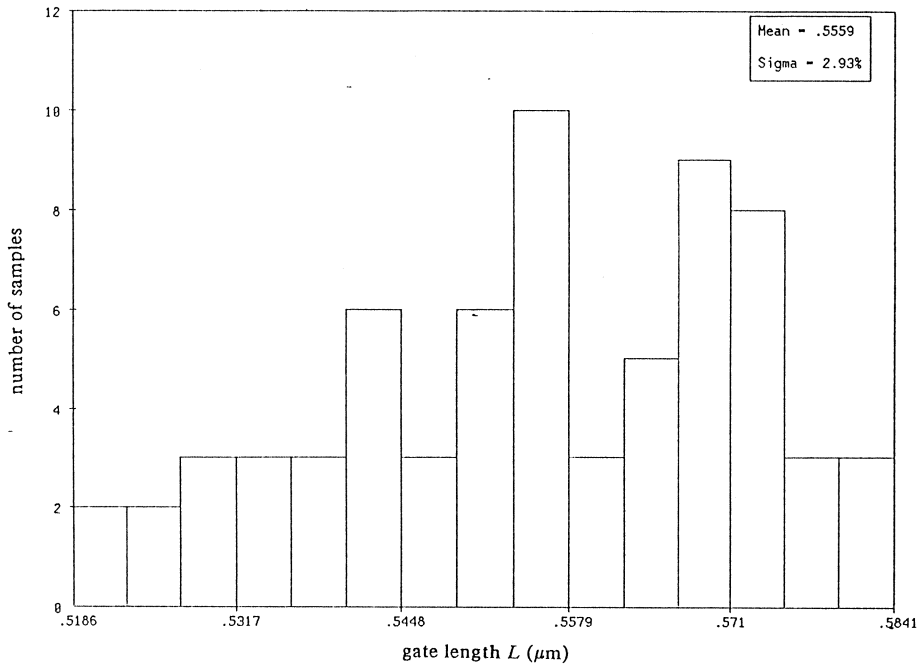

(a)

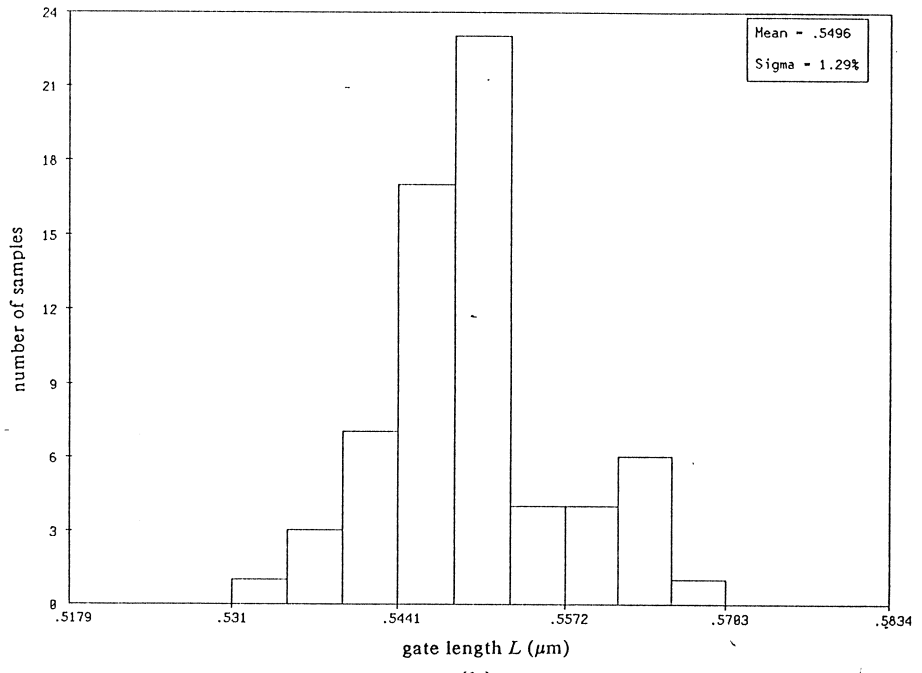

(b)

Fig. 13. Histograms of gate length L. (a) the Ladbrooke model. (b) the Khatibzadeh and Trew model.

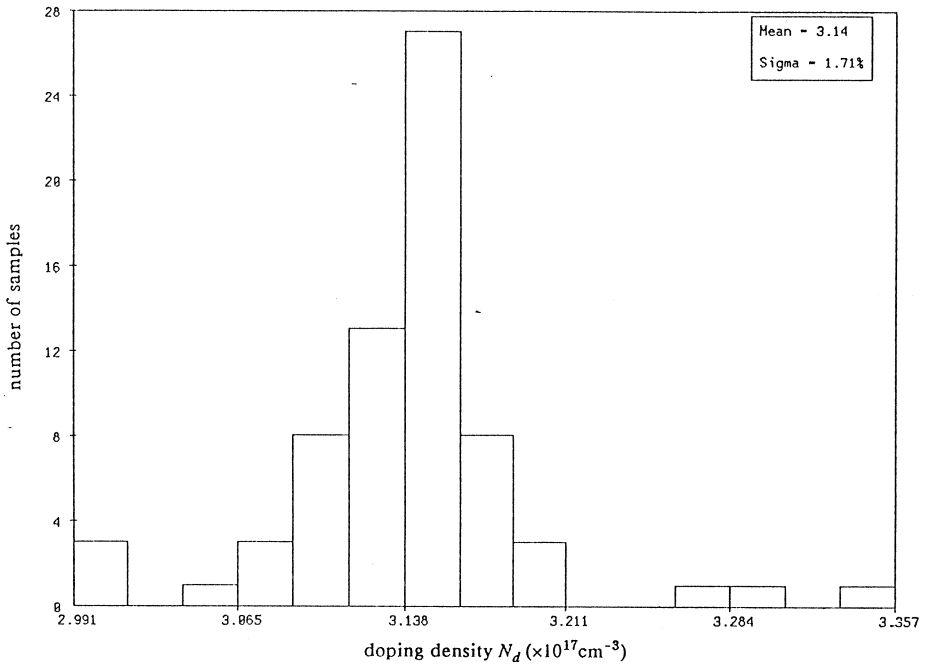

(a)

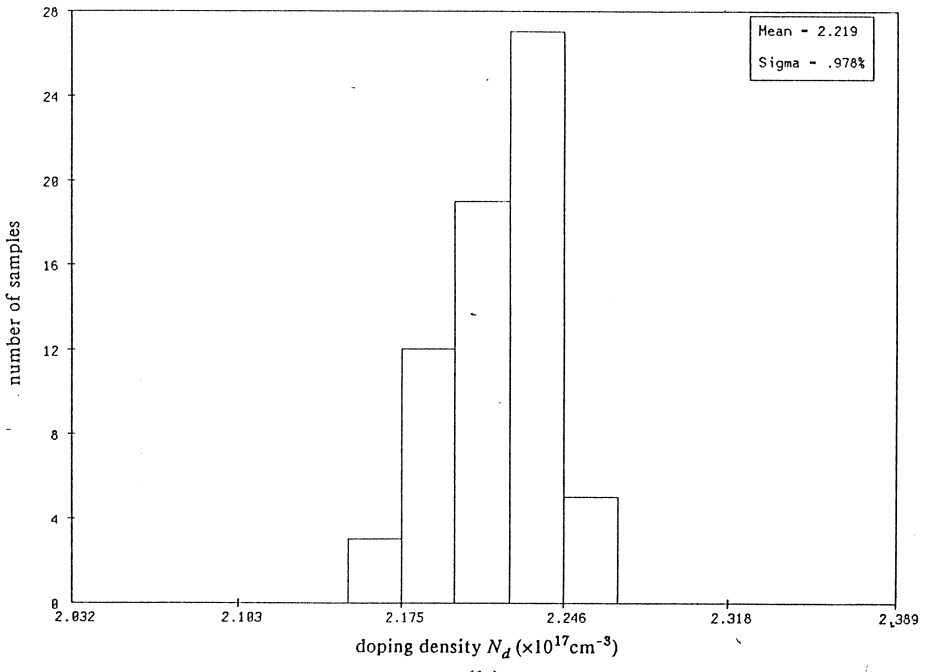

(b)

Fig. 14. Histograms of doping density N_d. (a) the Ladbrooke model. (b) the Khatibzadeh and Trew model.

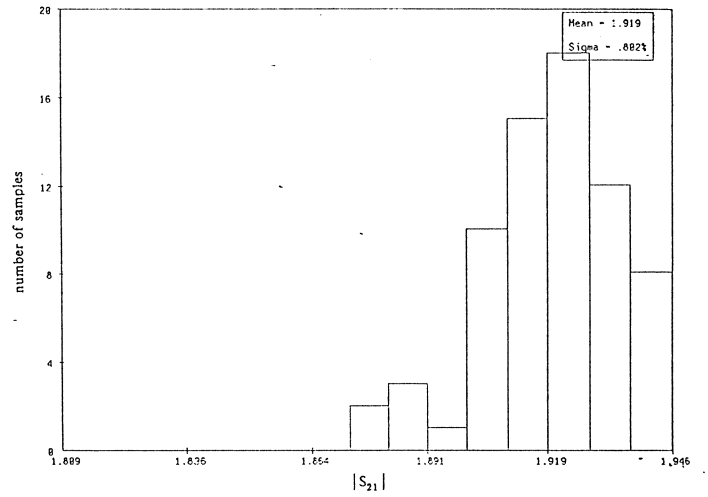

(a)

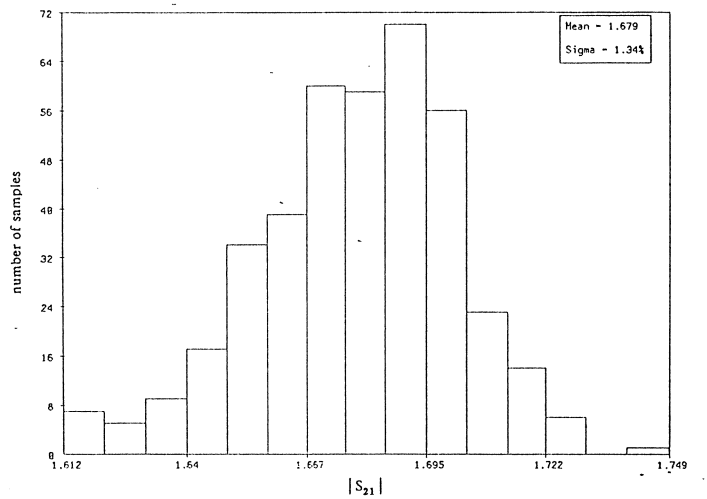

(b)

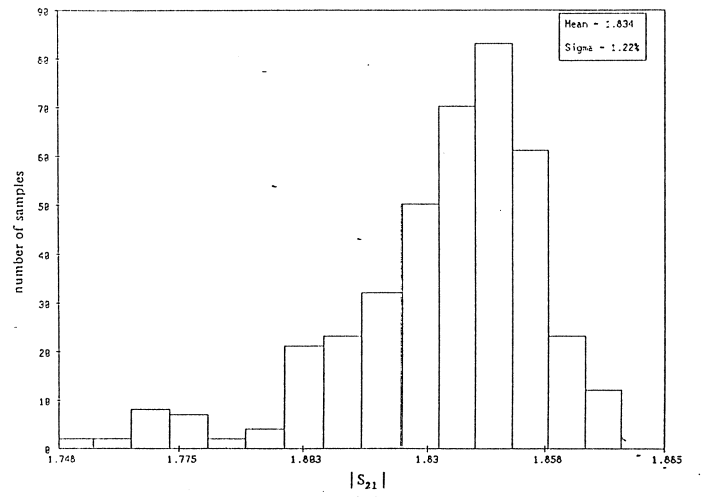

(c)

Fig. 15. Histograms of $|S_{21}|$ at V_{GS}=0V and V_{DS}=5V and at 11GHz from (a) measurements, (b) the Ladbrooke model, and (c) the Khatibzadeh and Trew model.

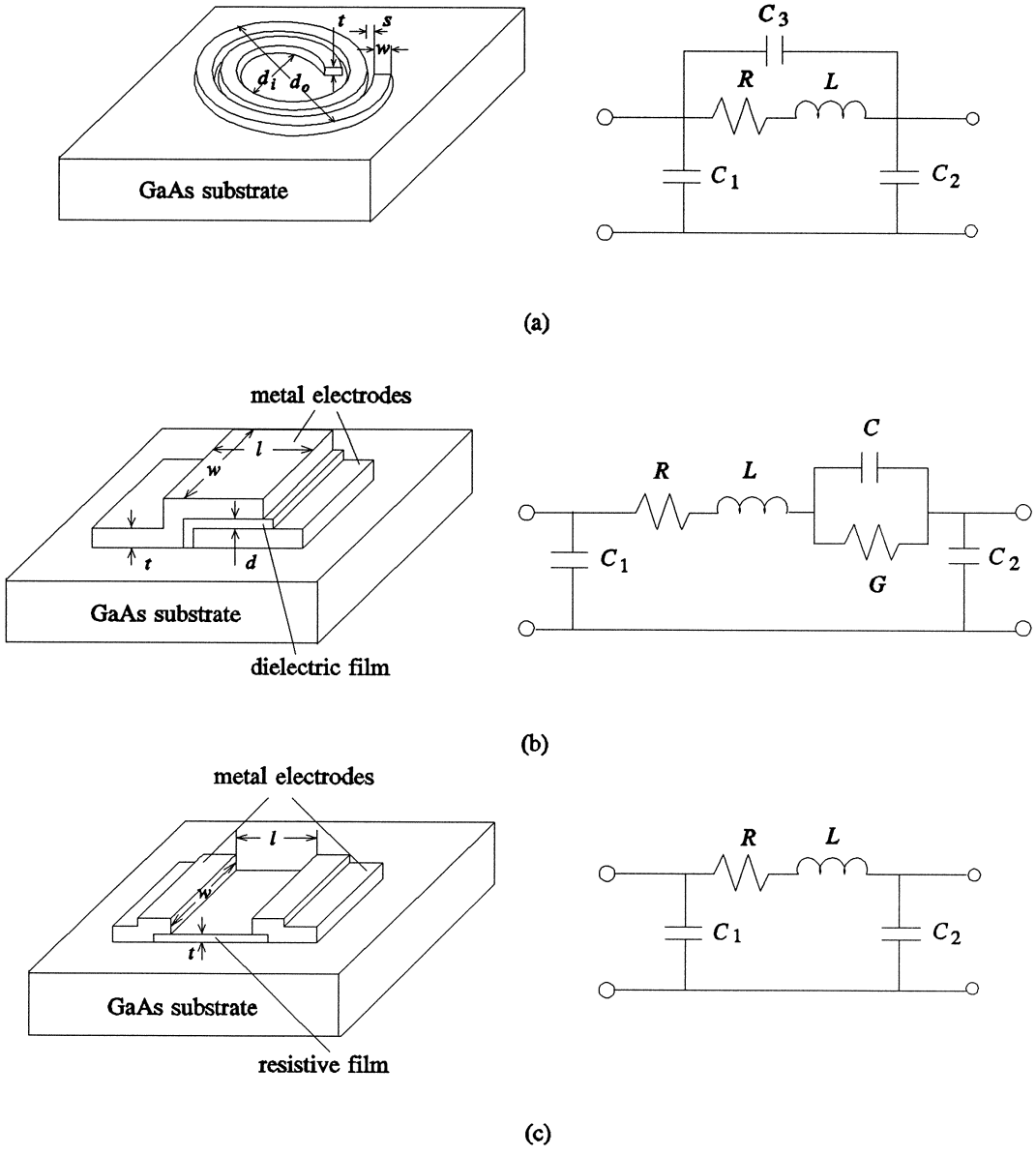

Fig. 16. Configuration of passive devices and their corresponding two port equivalent circuits [160]: (a) spiral inductor, (b) MIM capacitor and (c) planar resistor.

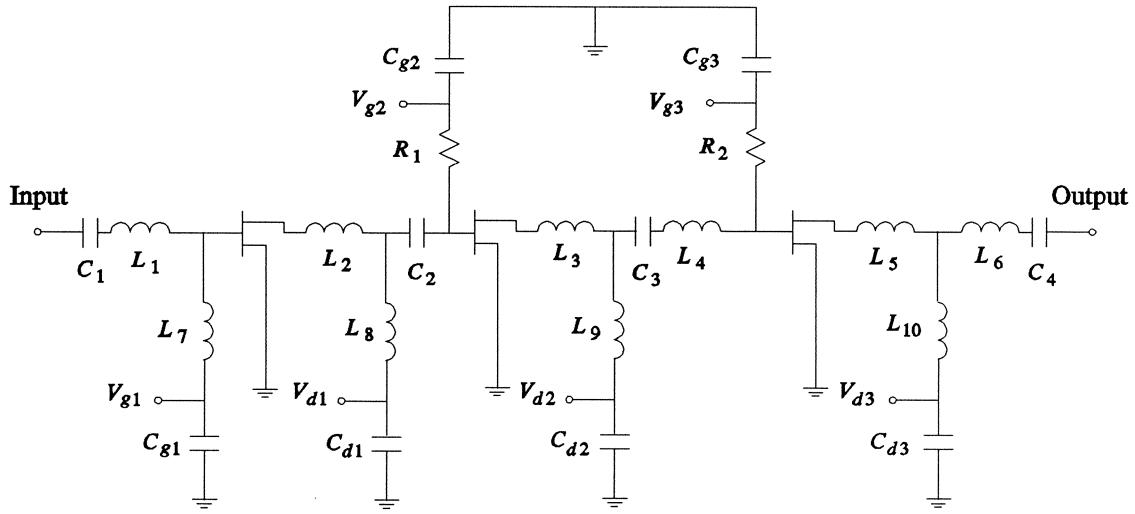

Fig. 17. Circuit diagram of X-band amplifier [163].

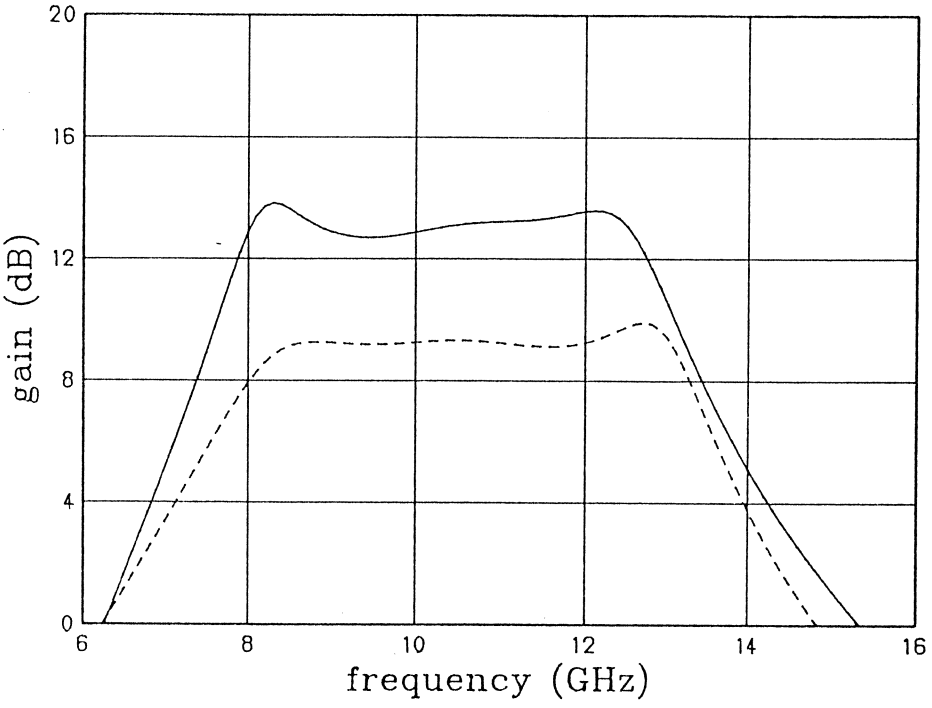

(a)

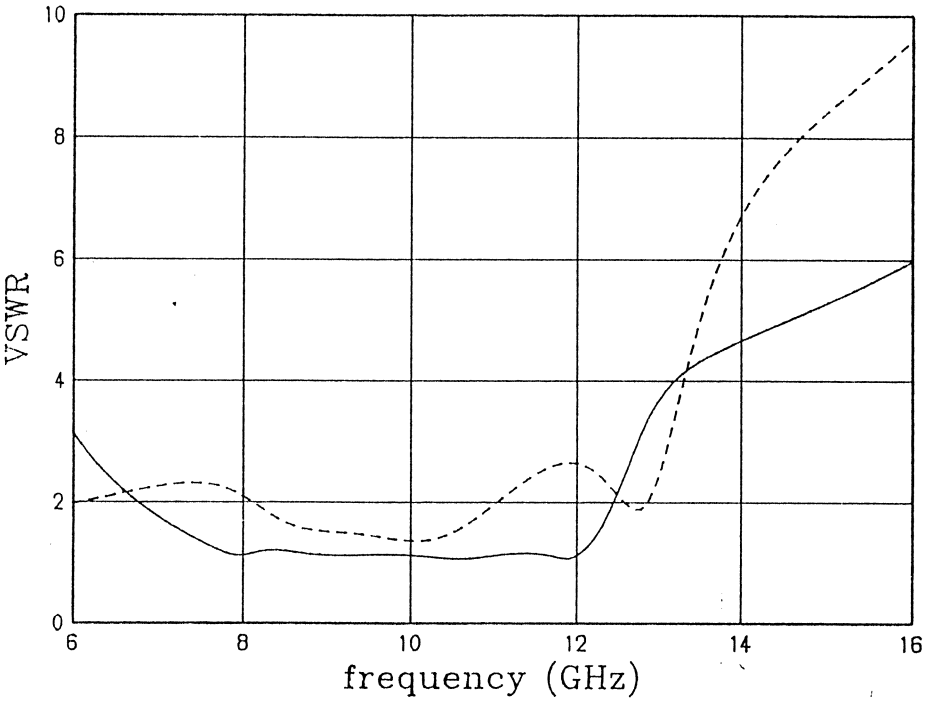

(b)

Fig. 18. (a) Gain and (b) VSWR versus frequency before (---) and after (——) nominal design optimization.

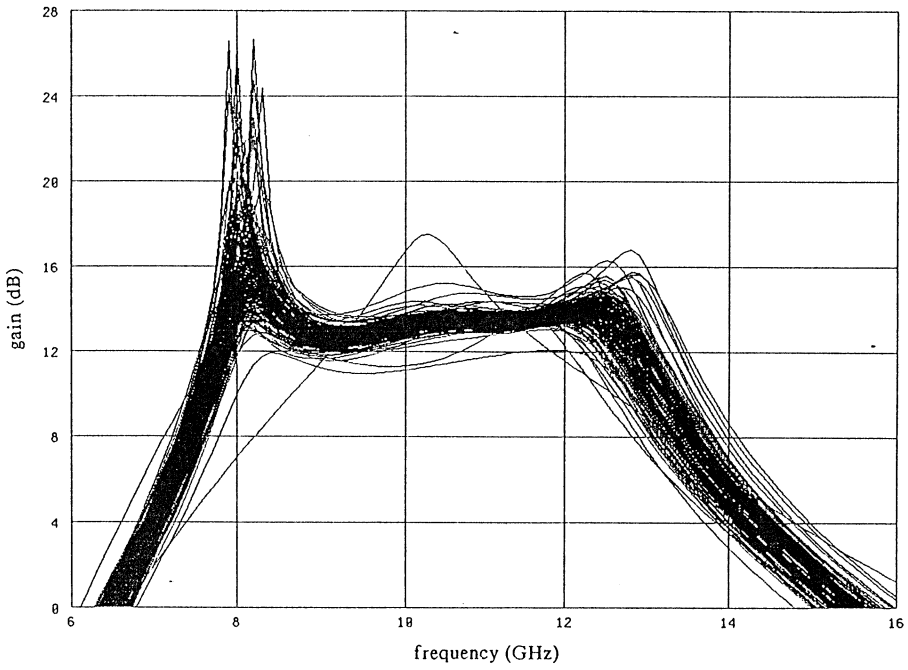

(a)

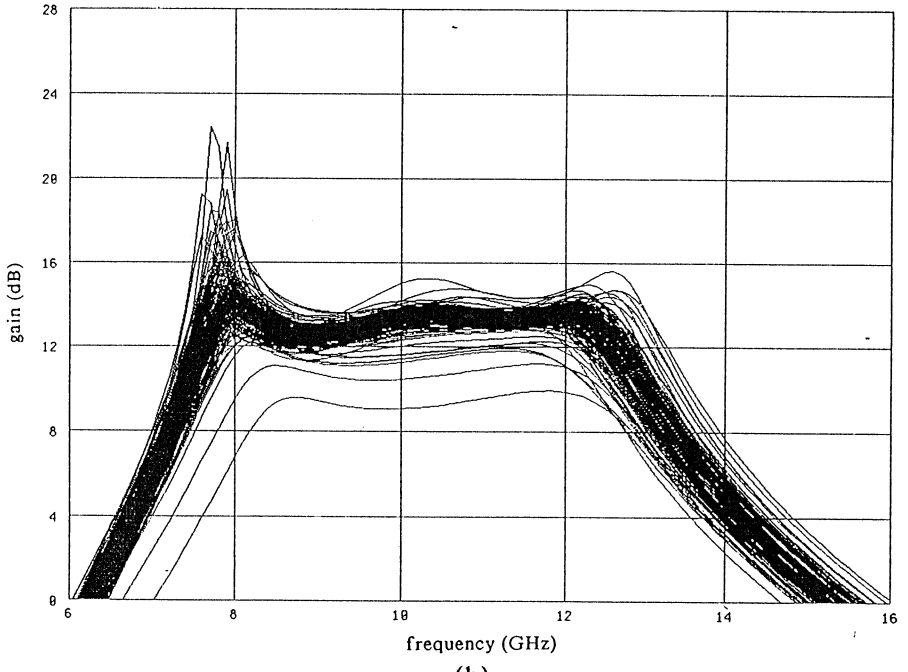

(b)

Fig. 19. Monte Carlo sweep of gain versus frequency (a) before and (b) after yield optimization.

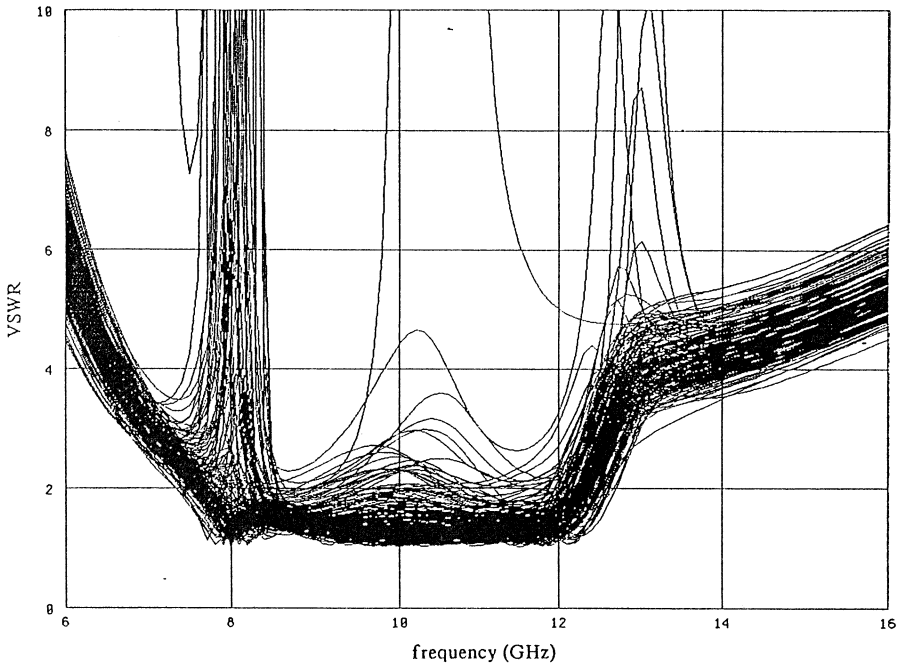

(a)

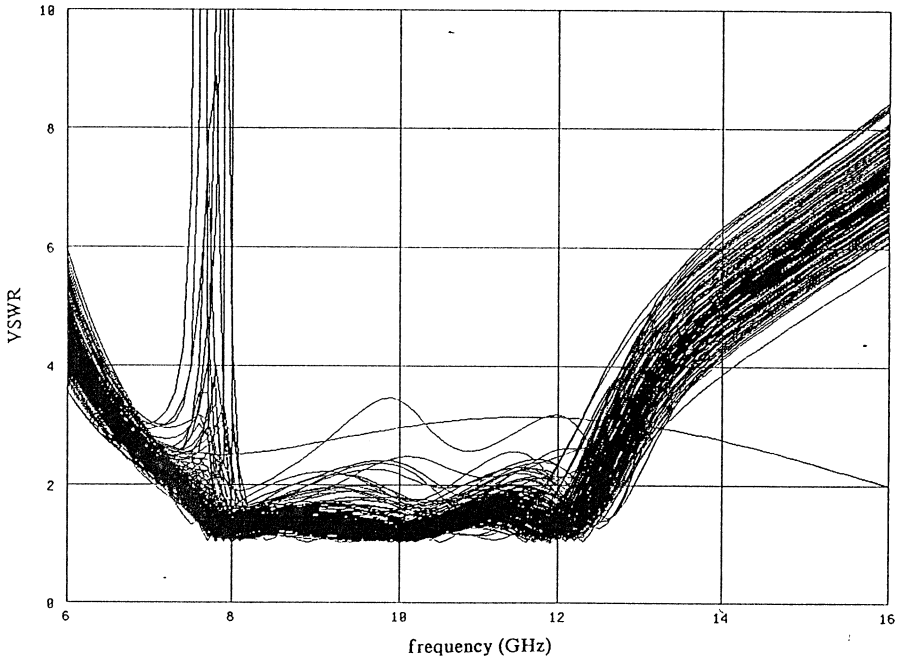

(b)

Fig. 20. Monte Carlo sweep of VSWR versus frequency (a) before and (b) after yield optimization.

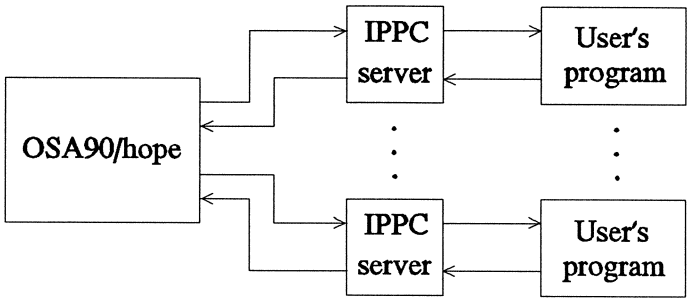

Fig. 21. Schematic diagram of Datapipe using inter-program pipe communication (IPPC), where user's programs may be user's in-house programs such as special purpose simulators, control programs, etc.

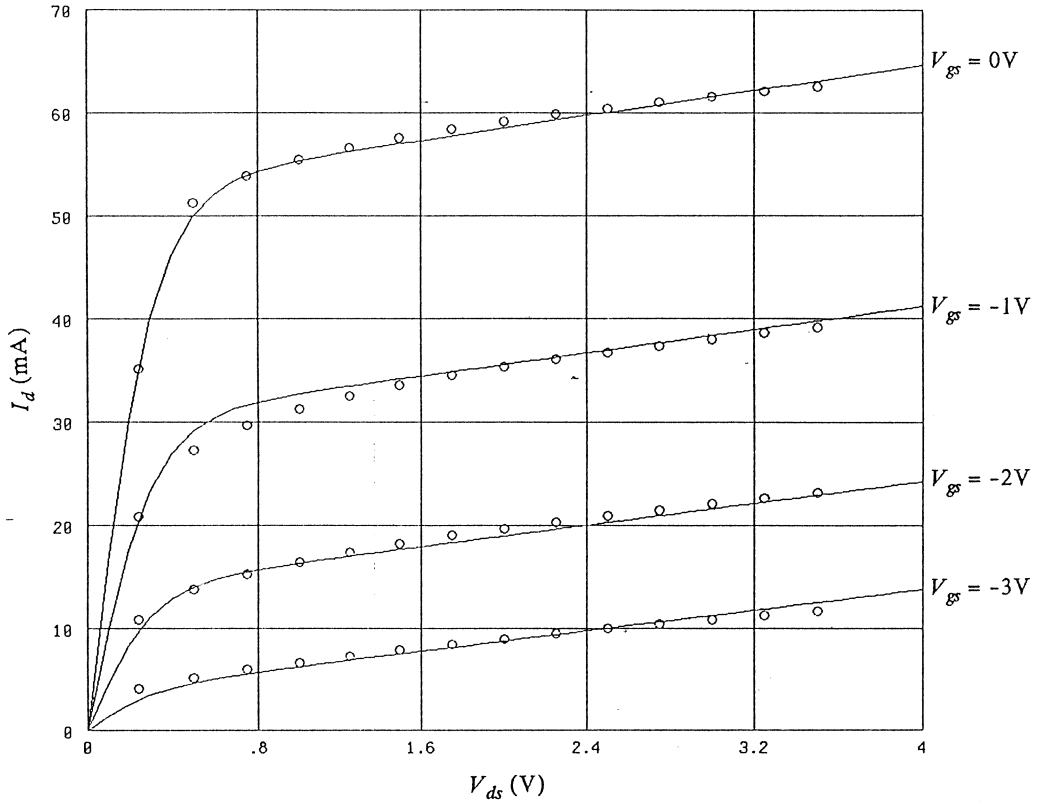

Fig. 22. Comparison of DC characteristics simulated by the 2D field-based simulator (O) and calculated by the Plessey model (——).